LMO7-dependent apical constriction requires the binding of the Myosin heavy chain

Miho Matsuda*, Chih-Wen Chu and Sergei Y. Sokol

Department of Cell, Developmental and Regenerative Biology, Icahn School of Medicine at Mount Sinai, New York, NY 10029, USA

*Corresponding author

Miho Matsuda

miho.matsuda@mssm.edu

Running title: Lmo7 regulates actomyosin contractility

Key words: Lmo7, actomyosin contractility, non-muscle myosin II, adherens junctions, morphogenesis, *Xenopus*

Abstract

The reduction of the apical domain, or apical constriction, is a process that occurs in a single cell or is coordinated in a group of cells in the epithelium. Coordinated apical constriction is particularly important when the epithelium is undergoing dynamic morphogenetic events such as furrow or tube formation. However, the underlying mechanisms remain incompletely understood. Here we show that Lim only protein 7 (Lmo7) is a novel activator of apical constriction in the *Xenopus* superficial ectoderm, which coordinates actomyosin contractility in a group of cells during epithelial morphogenesis. Like other apical constriction regulators, Lmo7 requires the activation of the Rho-Rock-Myosin II pathway to induce apical constriction. However, instead of increasing the phosphorylation of myosin light chain (MLC), Lmo7 binds muscle myosin II heavy chain A (NMIIA) and increases its association with actomyosin bundles at adherens junctions (AJs). Lmo7 overexpression modulates the subcellular distribution of Wtip, a tension marker at AJs, suggesting that Lmo7 generates mechanical forces at AJs. We propose that Lmo7 increases actomyosin contractility at AJs by promoting the formation of actomyosin bundles.

Introduction

Apical constriction is a cell shape change in which a cell reduces the size of its apical domain in the epithelium (Perez-Vale and Peifer, 2020; Sawyer et al., 2010). One consequence of apical constriction is cell ingression from the epithelium, a step that is sometimes required for epithelial-to-mesenchymal transition (EMT)(Martin and Goldstein, 2014; Ramkumar et al., 2016; Williams et al., 2012). Another consequence is epithelial invagination, a step leading to epithelial furrow or tube formation (Eiraku et al., 2011; Sherrard et al., 2010; Wallingford et al., 2013). Apical constriction is a fundamental cellular morphogenetic event during embryogenesis. Failure of apical constriction results in tissue/organ malformation such as a failure of neural tube closure (Colas and Schoenwolf, 2001).

Key regulators of apical constriction are actomyosin networks associated with adherens junctions (AJs) (Bresnick, 1999; Gorfinkiel and Blanchard, 2011). The actomyosin system consists of a highly dynamic network of filamentous actin (F-actin) cross-linked by non-muscle myosin II (NMII)(Vicente-Manzanares et al., 2009). Two NMII heavy chains (MYHs) assemble tail-to-tail and then oligomerize to form NMII bipolar filaments (Heissler and Sellers, 2014; Shutova and Svitkina, 2018). The head domain of NMII bipolar filaments binds F-actin and "walks" along F-actin. This sliding movement between F-actin and NMII generates contractile forces required for apical constriction (Lecuit et al., 2011; Martin and Goldstein, 2014; Salbreux et al., 2012).

Actomyosin networks can be organized in many patterns in a cell, from highly organized sarcomere-like actomyosin bundles to loose mesh-like networks (Agarwal and Zaidel-Bar, 2019; Schwayer et al., 2016). Highly organized circumferential actomyosin bundles have been observed in epithelial cells with constricted apical domain (Hildebrand, 2005; Martin, 2010; Pellegrin and Mellor, 2007). These actomyosin bundles are linked to AJs by F-actin binding proteins, such as αE-catenin, vinculin, ZO-1, EPLIN, and afadin (Abe and Takeichi, 2008; Drees et al., 2005; Gates and Peifer, 2005; Sawyer et al., 2009; Yamada et al., 2005).

Proteins that promote apical constriction usually act by recruiting or activating Rho-activated kinase (ROCK) at AJs, which then phosphorylates myosin regulatory light chain (MLC)(Amano et al.,

1996). For instance, RhoGEFs, such as p114RhoGEF and GEF-H1, increase the level of GTP-bound RhoA, which activates ROCK at AJs and induce apical constriction (Kolsch et al., 2007; Pathak and Dermardirossian, 2013; Terry et al., 2011). Epb41l5 binds and recruits p114RhoGEF to AJs (Nakajima and Tanoue, 2011; Nakajima and Tanoue, 2012). Shroom3 binds and recruits ROCK to AJs (Das et al., 2014; Nishimura and Takeichi, 2008). Downregulation of *gef-h1*, *epb41l5* or *shroom3*, as well as direct inhibition of MLC phosphorylation, leads to failure of apical constriction (Haigo et al., 2003; Hildebrand, 2005; Hildebrand and Soriano, 1999; Itoh et al., 2014; Lee et al., 2007). This confirms the importance of ROCK and MLC phosphorylation in apical constriction.

While MLC phosphorylation is required for apical constriction, it may not be sufficient, in particular for apical constriction leading to epithelial invagination. First, actomyosin contraction has to be synchronized for epithelial invagination (Alvarez and Navascues, 1990; Hardin and Keller, 1988; Kam et al., 1991; Martin et al., 2009; Sweeton et al., 1991). Second, contracting actomyosin bundles have to be tightly linked to AJs (Takeichi, 2014). Finally, actomyosin contraction has to be coupled with AJ remodeling between cells that are undergoing apical constriction with their neighbors. Defects in either of these processes lead to failure of apical constriction or epithelial invagination.

Previous studies identified mechanisms for synchronized apical constriction. For instance, Folded gastrulation (Fog) signaling is one of the few pathways dedicated to epithelial morphogenesis in insects (Benton et al., 2019). In *Drosophila fog* mutant embryos, fewer cells underwent apical constriction in the ventral furrow and posterior gut fold, and the spatial and temporal coordination of this process has been disrupted (Costa et al., 1994; Manning et al., 2013). Both Fog and Mesoderm invagination signal transducer (Mist), a secreted ligand and its G-protein coupled receptor (GPCR), activate RhoGEF2 and ROCK to define and coordinate apical constriction in a specific cell population (Gilmour et al., 2017; Manning and Rogers, 2014).

Another regulator of epithelial invagination is Canoe, the *Drosophila* homolog of vertebrate Afadin. Knockout of *canoe* resulted in severe defects in mesoderm invagination (Sawyer et al., 2009). *canoe* deficient cells initiated but did not complete apical constriction, with actomyosin bundles

coalescing into balls at the apical cortex (Sawyer et al., 2009). Afadin was proposed to promote F-actin association with AJs by directly binding to αE-catenin and F-actin (Sakakibara et al., 2020; Sawyer et al., 2009). While the Fog pathway is specific to insects, this Afadin function appears to be conserved in vertebrates, because *afadin* knockdown in mammalian cultured epithelial cells cancelled Shroom3-induced apical constriction (Sakakibara et al., 2020). This highlights the need of robust links between contracting actomyosin bundles and AJs for coordinated apical constriction in vertebrates.

These studies also emphasize the importance of feedback mechanisms between mechanical forces and actomyosin contractility at AJs. AJs sense mechanical forces generated by neighboring cells and change their own actomyosin contractility to accommodate changes occurring in neighboring cells. αE-catenin has been proposed to act as a mechanosensor at AJs. Tension-mediated conformation change of αE-catenin increases F-actin association with αE-catenin (Ishiyama et al., 2018; Seddiki et al., 2018; Yonemura et al., 2010). In a current model, however, increased F-actin association with AJs does not fully explain how a force-receiving cell increases its own actomyosin contractility in response to force. Increased pMLC, NMII bipolar filament formation, and the subsequent NMII incorporation into actomyosin bundles are required for actomyosin contractility. However, the underlying mechanisms remain incompletely understood.

In this study, we identify Lmo7 as a novel regulator of actomyosin contractility at AJs. While Lmo7 requires the activation of the Rho-ROCK-MyoII system to induce apical constriction, Lmo7 does not significantly increase MLC phosphorylation at AJs. Instead, Lmo7 directly binds NMIIA and increases NMIIA association with AJs. Lmo7 promotes the formation of thicker and denser actomyosin bundles and increases tension at AJs. Furthermore, Lmo7 induces collective cell movements in the *Xenopus* superficial ectoderm, suggesting that it coordinates actomyosin contractility in a group of cells for epithelial morphogenesis. We propose that Lmo7 increases actomyosin contractility at AJs by promoting the incorporation of NMII into actomyosin bundles, which is required for coordinated apical constriction for epithelial invagination.

Results

LMO7 localizes in close proximity to apical cell-cell junctions in *Xenopus* embryos

Lmo7 was originally identified as a binding protein of afadin and shown to localize at AJs in the epithelium in mice (Ooshio et al., 2004). We found that Lmo7 also localized at AJs in the superficial ectoderm in *Xenopus* embryos (Fig. 1A, B). Lmo7 localization differed from other components of AJs. First, Lmo7 formed two parallel lines along cell-cell boundaries, which were more evident in cell-cell boundaries with shorter lengths (arrowheads in Fig. 1Bb'). Other components of AJs, such as ZO1 that directly associates with transmembrane proteins claudin (Hartsock and Nelson, 2008), formed single-lines (Fig. 1C',D'). Further, ZO1 single-lines were located between Lmo7 double-lines (Fig. 1D-D"). Second, Lmo7 accumulated near but not in tricellular junctions (TCJs) (Fig. 1Bb"). These results suggest that Lmo7 localizes in close proximity to AJs.

AJs are closely associated with the apical circumferential actomyosin bundles (Yonemura et al., 1995). Based on the relative localization of Lmo7 and ZO1, we next asked whether Lmo7 locates within the apical circumferential actomyosin bundles. The major components of actomyosin bundles are F-actin, NMII and α-actinin, a member of the spectrin family that crosslinks antiparallel F-actin (Murphy and Young, 2015). We confirmed that both exogenously expressed GFP-NMIIA and GFP-α-actinin form two parallel lines along cell-cell boundaries in the *Xenopus* superficial ectoderm (Fig. 1E,F,S2A',B'). As seen in Lmo7, GFP-NMIIA was also excluded from TCJs (arrowheads in Fig. 1G-G").

In contrast, F-actin was observed in single-lines, although these F-actin single-lines appeared to be wider than ZO1 single-lines (compare Fig. 1D' and 1F'). The width of F-actin single-lines were almost the same as the width of GFP-Lmo7 double-lines (Fig. 1F-F"). These results confirm that there are two pools of F-actin, that differ in their incorporation into tightly formed actomyosin bundles at AJ. We found that double-lines formed by GFP-NMIIA or GFP-α-actinin largely overlapped with double-lines formed by Flag-Lmo7 (Fig. 1H-I", S2B-B"). Notably, Flag-Lmo7 double-lines appeared to be located slightly closer to the cell-cell boundary than GFP-NMIIA double-lines (arrowheads in Fig. 1I"). These results

suggest that Lmo7 localizes at actomyosin bundles associated with AJs.

Lmo7 induces apical constriction in *Xenopus* superficial ectoderm

A previous study showed that Smallish (Smash), a *Drosophila* homolog of Lmo7, induces apical constriction in follicular epithelial cells (Beati et al., 2018). To test whether vertebrate Lmo7 has a similar function, we overexpressed GFP-LMO7 in the superficial ectoderm of *Xenopus* embryos. Apical constriction was evaluated by the accumulation of pigment granules in the apical region of ectodermal cells as previously described (Haigo et al., 2003; Itoh et al., 2014; Morita et al., 2010; Ossipova et al., 2014). As we hypothesized, GFP-Lmo7 induced the accumulation of pigment granules (Fig. 2B,C). We further confirmed that Lmo7 did reduce the size of apical domain by phalloidin co-staining (Fig. 2L-L",M).

Next, we defined the domains of Lmo7 required for apical constriction. Lmo7 has the calponin homology (CH) domain, a domain evolutionally conserved among vertebrate Lmo7 and the Lmo7 homolog LIMCH1 (Fig. S4), the α-actinin binding domain, the PDZ domain, the coiled-coil domain and the LIM domain (Fig. 2A). Deletion mutant forms of Lmo7 illustrated in Fig.2A were expressed in the *Xenopus* superficial ectoderm and the accumulation of pigment granules was evaluated. We found that neither the N-terminal CH domain nor the C-terminal LIM domain were required for Lmo7-mediated accumulation of pigment granules (Fig. 2D,E). Further removal of the coiled-coil domain and the PDZ domain from the C-terminus did not affect Lmo7 ability to induce pigment granule accumulation (Fig. 2F). However, the removal of the evolutional conserved domain (compare Fig. 2D and 2G) or the α-actinin binding domain (compare Fig. 2F and 2H) diminished the ability of Lmo7 to induce pigment granule accumulation. Indeed, a GFP-Lmo7(a.a.242-709) deletion mutant containing the conserved domain and the α-actinin binding domain was sufficient to induce the accumulation of pigment granules (Fig. 2I), whereas the conserved domain (a.a. 242-476) itself did not show such activity (Fig. 2J). Since pigment granule accumulation by GFP-Lmo7(a.a.242-709) was rather weak (Fig. 2I), we further assessed

the apical domain size by phalloidin co-staining. We found that GFP-Lmo7(a.a.242-709), in fact, reduced the apical domain size (Fig. 2N-N",O). Lmo7(a.a. 242-476) did not induce apical constriction (Fig. 2O), suggesting that the evolutionally conserved domain is not sufficient to induce apical constriction. While GFP-Lmo7(a.a.1-709) strongly induced the accumulation of pigment granules, GFP-Lmo7(a.a.1-787) did not have this activity (compare Fig. 2F and Fig. 2K). Taken together, these results suggest that the evolutionally conserved domain and the α-actinin binding domain of Lmo7 are required for apical constriction and that the PDZ domain suppresses this Lmo7 activity.

Lmo7 localization at AJs is not sufficient to induce apical constriction

Lmo7 localized at AJ-associated actomyosin bundles and possibly in the space between actomyosin bundles and juxta-membrane components of AJs. Next, we asked whether this Lmo7 localization is required and/or sufficient to induce apical constriction. To test this, the subcellular distribution of Lmo7 deletion mutants were determined in the *Xenopus* superficial ectoderm. We found that all of the Lmo7 deletion mutants localized in close proximity to AJs or at least associated with the lateral membrane, while the degree of AJ association varied between mutants (Fig. S5). These results suggest that more than one domain of Lmo7 mediates its localization at AJs or associating actomyosin bundles. This distribution might be achieved by Lmo7 binding to α-actinin or afadin (Ooshio et al., 2004). Nevertheless, these results suggest that Lmo7 localization at AJs is not sufficient to induce apical constriction.

Lmo7 promotes the accumulation of F-actin at AJs

We investigated the mechanism underlying Lmo7-mediated apical constriction. Exogenously expressed GFP-Lmo7 formed two parallel lines along the cell-cell boundaries that overlapped double-lines formed by GFP-NMIIA or GFP-α-actinin (Fig. 1H-I",S2A-B"). We found that Lmo7 double-lines widened and intensified in AJs with higher expression of Lmo7 (compare cell-cell boundaries shown by

arrowheads (high-Lmo7) and those by arrows (low-Lmo7) in Fig. 3B). This wider and intensified accumulation of Lmo7 was accompanied by increased accumulation of F-actin which was also observed as double-lines along cell-cell boundaries (compare cell boundaries shown by arrowheads and arrows in Fig. 3B'). These results suggest that Lmo7 promotes the formation of dense, highly organized actomyosin bundles at AJs, leading to apical constriction.

Lmo7 requires activation of the Rho-ROCK-MyoII system to induce apical constriction

Previous studies showed that the Rho-ROCK-MyoII system controls actomyosin contractility for apical constriction (Martin and Goldstein, 2014). Accordingly, we asked whether LMO7-mediated apical constriction also requires the Rho-ROCK-MyoII system. To test this, we inhibited MLC phosphorylation in embryos expressing Lmo7. mRNA encoding Flag-Lmo7 was co-injected with mRNA encoding the dominant-negative form of ROCK (ROK-C) or the constitutive-active form of Mypt1 (Mypt1CA). Both have been shown to decrease MLC phosphorylation (Feng et al., 1999; Marlow et al., 2002; Weiser et al., 2009). We found that both ROK-C and Mypt1CA suppressed Lmo7-induced apical constriction (Fig. 3C-F). These results suggest that MLC phosphorylation is required for Lmo7-mediated apical constriction.

A major function of several proteins that induce apical constriction is to increase MLC phosphorylation at AJs (Hildebrand, 2005; Itoh et al., 2014; Nakajima and Tanoue, 2011). To evaluate whether Lmo7 acts similarly, we overexpressed it mosaically in superficial ectoderm cells. MLC phosphorylation was evaluated by the immunostaining for pMLC(Ser20), at the conserved phosphorylation site. In control cells, pMLC(S20) showed some enrichments at AJs and in the cytoplasm (Fig. 3G-G", H-H"). While Lmo7 reduced the cytoplasmic pMLC(S20), it did not increase the intensity of pMLC(S20) accumulation at AJs (Fig. 3H-H", I-I"). Even if there were some increases, the increase in pMLC(S20) at AJs was far less than F-actin enrichment at AJs in Lmo7-OE cells (Fig. 3A-B"). Lmo7 also did not increase pMLC(S20) by western blots (Fig. S6). These results suggest that while MLC phosphorylation is prerequisite for Lmo7-mediated apical constriction, Lmo7 may induce apical constriction downstream of MLC phosphorylation.

LMO7 binds myosin heavy chains, NMIIA and NMIIB

MLC phosphorylation initiates the formation of NMII bipolar filaments. These filaments then form oligomers that bind anti-parallel F-actin and form actomyosin bundles. If Lmo7 promotes apical constriction downstream of pMLC, one possibility is that Lmo7 facilitates NMII oligomer formation and/or NMII binding to F-actin after MLC phosphorylation, followed by the formation of denser and thicker actomyosin bundles. A previous study showed that a mouse LMO7 paralog LIMCH1 binds to the head domain of myosin heavy chain 9 (MYH9 or NMIIA) (Lin et al., 2017). We observed that the domain of Lmo7 required for apical constriction was conserved between Lmo7 and LIMCH1 (Fig. S4). This conserved domain is also in the region of LIMCH1 required for the NMIIA binding (Lin et al., 2017). Therefore, we hypothesized that Lmo7 binds NMIIA through the conserved domain and enhances NMIIA incorporation to actomyosin bundles at AJs.

To test LMO7-NMIIA interaction, Flag-Lmo7 was transiently expressed in HEK293 cells. Co-immunoprecipitation (IP) of endogenous NMIIA was assessed after lysate collection and IP using anti-Flag antibody. We also tested Lmo7-NMIIB (MYH10) interaction and found that Lmo7 binds to both NMIIA and NMIIB (Fig. 4A). As we hypothesized, the conserved domain a.a.(242-400), hereinafter referred to as NMII binding domain, was required and sufficient for Lmo7-NMIIA/B interaction (Fig. 4A).

Lmo7 recruits NMIIA to actomyosin bundles at AJs

Since the NMII binding domain of Lmo7 was required for Lmo7-mediated apical constriction (Fig. 2A), we asked whether Lmo7 binding to NMIIA/B increases NMII incorporation into actomyosin networks at AJs. We overexpressed Flag-Lmo7 in the superficial ectoderm and assessed the localization of endogenous NMIIA or exogenously expressed GFP-NMIIA/B. We found that Flag-Lmo7 significantly increased the accumulation of endogenous NMIIA at AJs (Fig. 4B-F"). Of note, the expression of Lmo7(AAAA) mutants, with substitutions in the NMIIA/B binding domain (underlined in Fig. S4), did

not increase NMIIA accumulation at AJs (Fig. S7). We further confirmed that Lmo7 induced the enrichment of exogenously expressed GFP-NMIIA at AJs (Fig. 4G-J").

In addition to increasing the intensity of NMIIA, Flag-Lmo7 also enhanced the width of NMIIA double-line, both for endogenous NMIIA (Fig. 4C-D") and for exogenously expressed GFP-NMIIA (Fig. 4H-I"). These denser and thicker NMIIA double-lines largely overlapped with Lmo7 double-lines while Lmo7 located closer to the cell-cell boundary (compare Fig. 4F-F" and Fig. 4J-J"). It should be noted that endogenous NMIIA showed more co-localization with Flag-Lmo7 (Fig. 4D-D") than exogenous GFP-NMIIA (Fig. 4I-I"). This difference might be explained by different antigen-binding sites (N-terminal GFP-tag vs anti-NMIIA antibody recognizing the C-terminal tail domain of NMIIA), sequence difference between mouse and *Xenopus* NMIIA, or the different levels of NMIIA expression. Nevertheless, our results strongly suggest that Lmo7 promotes the formation of NMIIA-containing actomyosin bundles at AJs. Interestingly, Lmo7 did not significantly increase the association of GFP-NMIIB with AJs, as compared to GFP-NMIIA (Fig. S8C-D"). Lmo7 also did not increase GFP-α-actinin enrichment at AJs (Fig. S8E-F"). These results suggest that Lmo7 specifically increases NMIIA incorporation with actomyosin bundles at AJs.

Lmo7 induces tension-dependent relocalization of Wtip

Lmo7 OE induced apical constriction, accompanied by the formation of denser and thicker actomyosin bundles containing NMIIA at AJs. The expected outcome of dense actomyosin bundle formation is contractile force generation. Therefore, we asked whether Lmo7 increases contractile force at AJs. A previous study showed that Shroom3 altered the distribution of Wtip, the Ajuba/Zyxin family protein, from dot-like structures to smooth lines at AJs (Chu et al., 2018). Cytoplasmic Wtip puncta also disappear in cells undergoing cytokinesis in which cortical tension is high (Chu et al., 2018). This indicates that the change of Wtip localization can be used as a readout of mechanical tension at AJs. To test whether Lmo7 increases tension, we expressed Flag-Lmo7 in a subpopulation of RFP-HA-Wtip expressing cell clusters in the *Xenopus* superficial ectoderm. As previously reported, RFP-HA-Wtip

formed intense dot-like structures near AJs in control wild-type cells (Fig. 5A-A",B-B"). Lmo7 eliminated these dot-like structures and promoted the formation of smooth lines along cell-cell boundaries (Fig. 5A-A",C-C"). Lmo7 also decreased dot-like structures in the apical domain (Fig. 5A-A"), however the physiological significance of these cytoplasmic dots requires further investigation. Nevertheless, these results suggest that Lmo7 may increase tension at AJs.

Lmo7-mediated apical constriction initiates epithelial invagination

One consequence of apical constriction is epithelial invagination during which a group of cells coordinate to reduce the size of apical domain, resulting in the epithelium changing shape. Lmo7 induces pigment granule accumulation at the apical region of *Xenopus* superficial ectodermal cells. In addition to that, we observed the alignment of cells with apically localized pigment granules, which appeared to connect two sites of mRNA microinjection (Fig. 6A). This suggests that Lmo7 has an ability to reduce the size of apical domain in a coordinated manner for collective cell movements.

To test this, we analyzed the collective movement of GFP-Lmo7-expressing cell clusters in live embryos. mRNA encoding GFP-Lmo7 was injected into two blastomeres of 4-cell stage embryos. A live embryo at St 11 was mounted in low-melting agarose for imaging (Fig. 6B). The center position of 26 individual cells expressing GFP-Lmo7 were marked by dots at the beginning of the imaging (red dots in Fig. 6A) and the end of the imaging (green dots in Fig. 6B). The overlay image of the embryo and relative position of red dots and green dots are shown in Fig. 6E and 6F. We found that there were four groups of cells showing distinctive collective movements: cells in group a and group b migrated toward the center of the imaging field, while cells in group c and group d migrated outward from the center of the imaging field (arrows in Fig. 6F). These results suggest that Lmo7 can direct collective cell movements in the epithelium during tissue-level morphogenesis.

Discussion

In this study, we showed that Lmo7 is a novel regulator of actomyosin contractility at AJs. Lmo7 promotes the formation of thicker and denser actomyosin bundles at AJs, leading to increased actomyosin contractility. While Lmo7 requires the activation of the Rho-ROCK-MyoII pathway to induce apical constriction, Lmo7 appears to function downstream of MLC phosphorylation. We also showed that Lmo7 binds to and recruits NMIIA to actomyosin bundles at AJs. We propose that Lmo7 promotes NMIIA incorporation into actomyosin networks, leading to the formation of denser and more organized actomyosin bundles required for proceeding apical constriction (Fig. 7).

The exact molecular mechanism of the Lmo7-mediated actomyosin bundle formation requires further investigation. After MLC phosphorylation, two MYHs assemble tail-to-tail, followed by NMII oligomer formation. These processes are negatively regulated by phosphorylation of MYHs (Conti et al., 1991; Dulyaninova et al., 2007; Even-Faitelson and Ravid, 2006; Murakami et al., 1998) or by the partner protein binding to the tail tip domain of MYHs (Dahan et al., 2012; Dulyaninova et al., 2005; Elliott et al., 2012; Garrett et al., 2006). It remains to be determined whether Lmo7 promotes NMII oligomer formation by decreasing phosphorylation of MYH or by inhibiting interaction between MYH and MYH binding proteins. Another possibility is that Lmo7 enhances MYH head domain function. It is likely that Lmo7 binds to the head region of NMIIA/B as described for Limch1 (Lin et al., 2017). The MYH head domain binds F-actin and works as a motor protein using myosin ATPase activity. Therefore, Lmo7 may increase MYH binding to F-actin and/or increase myosin ATPase activity.

Lmo7 appears to have an ability to induce apical constriction in groups of cells. Lmo7 OE in the *Xenopus* superficial ectoderm led to the accumulation of pigment granules. Pigment granules are apically localized and apical constriction of ectoderm cells can be measured as an increased density of pigment granules (Fesenko et al., 2000; Merriam et al., 1983). In addition to the apical accumulation of pigment granules, we observed a continuous line of pigments that appeared to form between two Lmo7 cell clusters derived from two independent injection sites. Furthermore, the live embryo imaging identified two distinct migratory behaviors of Lmo7-OE cells: inward cell movements that are parallel to a line

formed between two Lmo7 injection sites, and outward cell movements that are perpendicular to a line formed between two Lmo7 injection sites. These observations suggest that Lmo7 has an ability to direct collective movements in the epithelium. Further characterization of cell behaviors is needed to understand how Lmo7 coordinates apical constriction.

Lmo7 dramatically increased NMIIA enrichment at AJs. The multivalent nature of Lmo7 protein might contribute to this NMIIA enrichment and dense actomyosin bundle formation at AJs. Recent studies showed that ZO proteins, which are multi-domain containing proteins at tight junctions (TJs), have properties of liquid-liquid phase separation (LLPS)(Beutel et al., 2019; Schwayer et al., 2019). Lmo7 binds to NMIIA, α-actinin, afadin and possibly F-actin through four independent domains. Lmo7 itself shows intense accumulation at AJs as seen for ZO proteins at TJs. It is possible that Lmo7 has properties similar to ZO proteins and work as a platform that increases local concentrations of Lmo7 and Lmo7-interacting proteins. This Lmo7 property might be important for denser and thicker actomyosin bundle formation.

Despite substantial effects of Lmo7 on the actomyosin organization, knockout of *lmo7* had little effect during mouse embryogenesis. *lmo7* knockout mice were viable and developed normally, except that they had increased susceptibility to spontaneous lung cancer in the adulthood (Lao et al., 2015; Tanaka-Okamoto et al., 2009). *lmo7* deficiency also caused cuticular plate deficiencies, including reduced F-actin density and abnormal stereocilia rootlets in the mouse inner ear (Du et al., 2019). These studies show that while Lmo7 is essential for AJ and/or actomyosin organization in some tissues, Lmo7 function is largely compensated by other proteins in other tissues in vertebrates. This compensation might be mediated by the Lmo7 paralog, LIMCH1 (Lin et al., 2017). However, *Drosophila* mutants of *smash,* the only homolog of vertebrate Lmo7/LIMCH1, failed mesoderm invagination (Beati et al., 2018). Double knockout of Lmo7 and LIMCH1 might be necessary to evaluate loss of function effects of Lmo7/LIMCH1 in vertebrates.

It has been proposed that mechanical force generation and transmission plays a central role in epithelial morphogenesis. AJs contain proteins that generate mechanical forces as well as sense and

transmit mechanical forces. Lmo7 is a novel regulator of actomyosin contractility at AJs and generates mechanical forces by increasing actomyosin contractility. In addition to generating mechanical forces, Lmo7 may also be involved in sensing and transmitting mechanical forces at AJs. Lmo7 binds afadin (Ooshio et al., 2004) and afadin binds αE-catenin, a well-known mechanosensor at AJs . It would be interesting to determine how Lmo7, afadin and αE-catenin interplay to effectively generate, sense and transmit mechanical forces to orchestrate collective movements for epithelial morphogenesis.

Materials and Methods

Plasmids

Xenopus laevis Lmo7 was obtained from Dharmacon. Full-length and truncated forms of Lmo7 were PCR amplified using Choice Taq DNA polymerase (Denville Scientific) and cloned into a pCS107 expression vector by standard molecular biology protocols using restriction enzymes (New England Biolabs) and Mighty Mix DNA ligation kit (Takara). Primers used for PCR amplification are in Supplemental Table 1. pCS2-GFP-NMIIA, pCS2-GFP-NMIIB and pCS2-α-actinin 4 were subcloned from pCMV-NMIIA, pCMV-NMIIB and pCS2-TSMod-α-actinin 4, kindly provided by Dr. Adelstein and Dr. Michiue (Yamashita et al., 2016). pCS2-ROK-C and pCS2-Mypt1CA were kindly provided by Dr. Marlow (Marlow et al., 2002) and Dr. Kimelman (Weiser et al., 2009). Plasmid DNA were purified using Qiagen Plasmid Midi kit (Qiagen). Prior to *in vitro* transcription, plasmid DNA was linearized by restriction enzymes.

Xenopus husbandry

Wild-type *Xenopus laevis* adults were purchased from Nasco, maintained and handled according to the recommendations in the Guide for the Care and Use of Laboratory Animals of the National Institutes of Health. A protocol for animal use was approved by the Institutional Animal Aare and Use Committee (IACUC) at Icahn School of Medicine at Mount Sinai. *In vitro* fertilization was performed as described previously (Dollar et al., 2005).

Microinjection of *in vitro* synthesized mRNA

Embryo staging was determined according to Nieuwkoop and Faber (1967). For microinjections, embryos were transferred into 3% Ficoll 400 (Pharmacia) in 0.5× Marc's modified Ringer's (MMR) solution (50 mM NaCl, 1 mM KCl, 1 mM CaCl2, 0.5 mM MgCl2 and 2.5 mM HEPES (pH 7.4))(Peng, 1991). Linearized plasmid DNA was used to synthesize mRNA using mMessage mMachine SP6 or T7

Transcription kit (Invitrogen). Synthesized mRNA was purified by LiCl precipitation. mRNA in 5-10 nl RNase free water was microinjected into one or two blastomeres of four to sixteen cell stage embryos. The amounts of injected mRNA per embryo are indicated in the figure legends.

Cell culture and transfection

HEK293 cell line was purchased from ATCC and maintained in Dulbecco's modified eagle media (DMEM) (Corning) supplemented with 10% fetal bovine serum (Sigma) in a 37C incubator with 5% CO2. HEK293 cells grown in 60 mm dish at 70-80% density were transfected with a mixture of 4 ng plasmid DNA and 20 ng DNA Polyethylenimine (PEI)(Polysciences). Cell lysates were extracted 24 hours after transfection.

Immunoprecipitation and western blots

Cell lysates were extracted from HEK293 cells using RIPA buffer (50 mM Tris-HCl pH 7.4, 150 mM NaCl, 1% NP-40, 0.5% sodium deoxycholate, 0.1% SDS) supplemented with Protease Inhibitor Cocktail III (Calbiochem) and PhosStop phosphatase inhibitor cocktail (Roche). Cell lysates were incubated with anti-Flag M2 agarose (Sigma) at 4˚C for at least 6 hours. Agarose beads were washed three times in Tris-buffered saline containing 0.05% Triton X-100 (TBST). Agarose beads were heated at 95˚C for 5 min in SDS sample buffer containing 5% β-mercaptoethanol (Sigma). After SDS-PAGE and transfer to a nitrocellulose membrane with a 0.2 μm pore size (RioRad), western blots were performed. Antibodies used are the following: rabbit anti-NMIIA pAb (BioLegend, #POLY19098, 1:500), rabbit anti-NMIIB pAb (BioLegend, #POLY19099, 1:500), mouse anti-DYKDDDDK mAb clone 2H8 (Cosmo Bio USA, #KAL-K0602, 1:1,000) and mouse anti-GFP mAb clone B2 (Santa Cruz Biotechnology, #sc-9996, 1:500). HRP-conjugated secondary antibodies against mouse or rabbit IgG are obtained from Cell Signaling technology (#7074, #7076, 1:5000). Chemiluminescent signals were acquired using Clarity ECL Western Blotting Substrates (Bio-Rad) on ChemiDoc MP Imaging System (Bio-Rad).

Xenopus embryo lysate extraction and western blots

10-20 embryos were incubated in lysis buffer (50 mM Tris-HCl (pH 7.6), 50 mM NaCl, 1 mM EDTA, 1% Triton X-100) supplemented with protease inhibitor and protein phosphatase inhibitor cocktails as described above. After centrifugation for 3 min at 16,000 g, the supernatant was mixed with SDS-sample buffer, followed by standard SDS-PAGE and western blot protocol. Experiments are repeated at least three times.

Examination of apical constriction

mRNA encoding Lmo7, ROK-C or Mypt1-CA were injected into two animal ventral blastomeres of 4-cell stage embryos. Embryo images were captured using a Leica stereo microscope equipped with CCD camera. The accumulation of pigment granules was assessed based on the density of pigments. Each experiment included 20-30 embryos per condition. Experiments are repeated at least three times.

Whole-mount Immunocytochemistry

For formaldehyde fixation, *Xenopus* embryos were devitellinized manually using forceps and fixed in MEMFA (0.1 M MOPS (pH 7.4), 2 mM EGTA, 1 mM MgSO4, and 3.7% formaldehyde)(Harland, 1991) for 60 min at room temperature (RT). After wash in phosphate buffered saline (PBS), embryos are permeabilized in 0.1% Triton in PBS for 30 min. For trichloroacetic acid (TCA) fixation, devitellinized embryos were fixed in ice-cold 10% TCA for 30 min. Embryos were then incubated in 1% BSA in TBS at 4C overnight for blocking. After that, embryos were incubated with primary antibodies in 1% BSA, 1% DMSO in PBS or TBS at 4C overnight. Antibodies used in this study are the following: rabbit anti-NMIIA pAb (BioLegend, #POLY19098, 1:300), mouse anti-DYKDDDDK mAb clone 2H8 (Cosmo Bio USA, #KAL-K0602, 1:500), rat anti-HA mAb clone 3F10 (Roche, 118673230002, 1:100), and chicken anti-GFP pAb (abcam, #ab13970, 1:500). After wash in PBS or TBS three times, embryos were incubated with secondary antibodies conjugated with either Alexa 488, Cy3 or Cy2 fluorescent dyes in 1% BSA,

1% DMSO in PBS at 4C overnight. Alexa 488, Cy3, or Cy2-conjugated secondary antibodies against mouse, rat and rabbit IgG or chicken IgY are obtained from Invitrogen (#A-32723, #A-11034, 1:300) or Jackson ImmonoResearch Laboratory (#711-165-152, #715-165-151, #712-165-153, #703-225-155, 1:500). AlexaFlur 555-phalloidin (Invitrogen, A34055) was added to label F-actin to secondary antibody solution when necessary. After wash in PBS or TBS three times, embryos are transferred in 25% glycerol in PBS. The animal pole side of embryos was dissected manually by forceps and mounted on slide glasses using Vectashield mounting medium. (Vector). 4% PFA in PBS overnight at 4˚C. Zeiss AxioImager upright microscope equipped with Zeiss Axiocam CCD camera or Zeiss LSM880 confocal microscope system was used for imaging. Images were captured from at least 5 independent embryos. Experiments are repeated at least three times. Captured images were processed and quantified using ImageJ software.

Time-lapse imaging of *Xenopus* embryos

mRNA encoding GFP-Lmo7 were injected into two blastomeres in 4-cell stage embryos. Approximately at St 9, embryos were mounted in 1% SeaPlaque low-melting agarose (Lonza) in 0.1x MMR. Time-lapse images were taken on a Zeiss AxioZoom microscope equipped with a Zeiss Axiocam CCD camera at 20 min intervals for 6 hours. Images were processed and quantified using ImageJ software.

Quantification and statistical analyses

Quantification of fluorescence signals was performed by analyzing individual single plane images. Integrated fluorescence intensity of immunostaining was measured using an ImageJ plugin. The Student's t-test was used to test association of continuous variables. The Chi-squared test was used to test categorical variables.

Acknowledgements

We thank Dr. R. Adelstein and T. Michue for plasmids, Pamela Mancini for help with Lmo7 mutagenesis at the early stages of this project. We thank members of Dr. Sokol's laboratory for discussion and

comments on the manuscript. This research was supported by the NIH grant R35GM122492 to SYS.

Competing Interests

No competing interests declared

Funding

This work was supported by the National Institutes of Health grant R35GM122492 to SYS.

Data availability

n.a.

Figure legends

Figure 1

Lmo7 localizes in actomyosin bundles associated with AJs

(A) GFP-Lmo7 localization at AJs in the *Xenopus* superficial ectoderm at St 11. An area marked by a dotted rectangle in A is enlarged in B. (B) GFP-Lmo7 forms double-lines near AJs. Areas marked by dotted rectangles in B are enlarged in b' and b". (b') GFP-Lmo7 double-lines are more evident in shorter cell-cell junctions. (b") Enrichment of GFP-Lmo7 near tricellular junctions (TCJs). GFP-Lmo7 is excluded from TCJs. (C-C") Relative localization of GFP-Lmo7 and RFP-ZO1 at AJs in the *Xenopus* superficial ectoderm at St 11. An area marked by a dotted rectangle in C is enlarged in D. (D-D") GFP-Lmo7 and RFP-ZO1 do not co-localize at AJs. RFP-ZO1 single line is located between GFP-Lmo7 double-line. (E-E") Relative localization of GFP-NMIIA and F-actin in the *Xenopus* superficial ectoderm at St 11. The area marked by dotted rectangles in E is enlarged in F and in G. (F-F") GFP-NMIIA is observed as a double-line, whereas phalloidin is observed as a thick single-line. The GFP-NMIIA double-line largely overlaps with the phalloidin single-line. (G-G") GFP-NMIIA is enriched near TCJs but excluded from TCJ (arrowheads). (H-H") Relative localization of Flag-Lmo7 and GFP-NMIIA in the *Xenopus* superficial ectoderm at St 11. An area marked by a dotted rectangle in H is enlarged in I. (I-L") Flag-Lmo7 double-line overlaps with the GFP-NMIIA double-line, while the Flag-Lmo7 double-line is localized slightly closer to cell-cell boundaries.

Figure 2

Lmo7 induces apical constriction in the *Xenopus* superficial ectoderm

(A) Schematics of Lmo7 domain structures. Lmo7 has the N-terminal CH domain, the evolutionally conserved domain, the α-actinin binding domain, the PDZ domain, two coiled-coil domains and the C-terminal LIM domain. Deletion mutants used in this study are illustrated. (B-K) Accumulation of pigment granules in the *Xenopus* superficial ectoderm at St 11. GFP-tagged full-length Lmo7 (C), Lmo7(ΔCH)(D), Lmo7(ΔLIM)(E), and Lmo7(a.a.1-709)(F) induced the accumulation of pigment

granules. Further deletion of the evolutionally conserved domain (G) or the α-actinin binding domain (H) depleted the Lmo7 ability to induce the accumulation of pigment granules. Lmo7(aa. 242-709) containing the evolutionally conserved and the α-actinin binding domain induces the accumulation of pigment granules (I), while the evolutionally conserved domain alone does not (J). The PDZ domain inhibits the Lmo7 function to induce pigment granule accumulation (K). (L-L") GFP-Lmo7 OE reduces the apical domain size in the *Xenopus* superficial ectoderm in St 11. GFP-Lmo7 was expressed in mosaic. Embryos are co-stained with phalloidin. (M) Quantification of apical domain size in cells expressing GFP-Lmo7 (N-N") GFP-Lmo7(a.a. 242-709) OE reduces the apical domain size in the *Xenopus* superficial ectoderm in St 11. GFP-Lmo7(a.a. 242-709) was expressed in mosaic. Embryos are co-stained with phallodin. (O) Quantification of apical domain size in cells expressing GFP-Lmo7(a.a. 242-709) or GFP-Lmo7(a.a. 242-409). Images were taken of >5 embryos. Apical domain size was measured only in cells that shared at least one cell-cell boundary with non-GFP expressing control cells and GFP-Lmo7 or Lmo7 deletion mutants. *<0.0001.

Figure 3

Lmo7 promotes the formation of thicker and denser actomyosin bundles at AJs through the activation of the Rho-ROCK-MyoII pathway.

(A) The accumulation of F-actin in Flag-Lmo7 OE cells in *Xenopus* superficial ectoderm. Flag-Lmo7 was expressed in mosaic. Embryos were co-stained with phalloidin at St 11. An area marked by a dotted rectangle is enlarged in B. (B-B') Increased Lmo7 expression is associated with the formation of thicker and denser F-actin bundles. Arrowheads indicate AJs with high Lmo7 expression and high phalloidin enrichment. Arrows indicate AJs with low Lmo7 expression and low phalloidin enrichment. (C-F) Lmo7-mediated apical constriction requires the activation of the Rho-ROCK-MyoII pathway. Flag-Lmo7 was co-expressed with the dominant-negative form of ROCK (ROK-C) or the constitutive active form of Mypt1 (Mypt1CA). Co-expression of ROCK-C or Mypt1CA suppresses Lmo7-induced accumulation of

pigment granules (E,F). (G-G') Lmo7 OE does not significantly increase the level of pMLC(S20) at AJs. Flag-Lmo7 was overexpressed in mosaic in *Xenopus* superficial ectoderm. Embryos were immunostained with anti-pMLC(S20) at Stage 11. (H-I") Enlarged images of G-G". Immunostaining of anti-pMLC(S20) antibody in control wild-type cells (H-H") or cells expressing Lmo7 (I-I"). (J-J') Overexpression of Lmo7(AAAA) mutant which has mutations in the conserved WQ-WK sequence (shown in Fig. S4) does not increase the level of pMLC(S20) at AJs.

Figure 4

Lmo7 binds and recruits NMIIA to AJs, leading to thicker actomyosin bundle formation at AJs

(A) Lmo7 binds NMIIA and IIB through the evolutionally conserved domain. Flag-tagged full-length and deletion mutant forms of Lmo7 were transiently expressed in HEK293 cells. At 24 hours post transfection, cell lysates were mixed with anti-Flag M2 agarose for immunoprecipitation (IP). Co-immunoprecipitaion of endogenous NMIIA and NMIIB was assessed by western blots. Asterisks indicate bands corresponding to undegraded full-length or deletion mutant forms of Lmo7. (B-B") Lmo7-OE increases the enrichment of endogenous NMIIA at AJs in the *Xenopus* superficial ectoderm at St 11. A dotted square in B' is enlarged in C. Dotted squares in B-B" are enlarged in D-D". (C) Endogenous NMIIA is weakly associated with AJs in non-Lmo7 expressing control cell. (D-D") Flag-Lmo7 increases the accumulation of endogenous NMIIA at AJs. (E-F") Further enlargement of C-D". Flag-Lmo7 OE increases the intensity and the width of NMIIA double line. Lmo7 localizes closer to cell-cell boundaries than NMIIA. (G) GFP-NMIIA localizes at AJs. A dotted square is enlarged in I. (H-H") Co-expression of Flag-Lmo7 promotes the accumulation of GFP-NMIIA. A dotted square is enlarged in J. (I) The localization of exogenously expressed NMIIA in non-Lmo7 expressing control cells. (J-J") Flag-Lmo7 increases the accumulation of exogenously expressed GFP-NMIIA at AJs.

Figure 5

Lmo7 changes the localization of RFP-Wtip at AJs, a readout of mechanical tension

(A) Lmo7 OE eliminated RFP-Wtip puncta both in the cytoplasm and at cell-cell junctions. Flag-Lmo7 was expressed in mosaic in subpopulation of RFP-Wtip expressing cell clusters (shown by asterisks). Areas of dotted rectangles are enlarged in B and C. (B-B") RFP-Wtip forms puncta at cell-cell junctions in cells not-expressing Flag-Lmo7. (C-C") Flag-Lmo7 OE eliminates RFP-Wtip puncta formed near AJs. RFP-Wtip single-line is located between Flag-Lmo7 double-lines.

Figure 6

Lmo7 induces collective cell movements in the *Xenopus* ectoderm

(A) Lmo7-OE induces the formation of the line enriched with pigment granules. Arrowheads indicate the approximate location of the injection sites. (B) A fluorescent image of a whole *Xenopus* embryo expressing GFP-Lmo7 at St 11. The animal pole view. (C-E) Images of GFP-Lmo7 expressing embryos at 0 h (A) and 3 hours later of the same embryo (B). Overlay of these two images is shown in C. The center positions of 25 cells are marked by red dots (A) and green dots (B). (F) An overlayed image of red dots and green dots from C and D. Cells' movements were divided into four groups. Cells in group a and b locate near the central rod region of the indentation and migrate toward the indentation. Cells in group c and d locate near the end region of the indentation and migrate away from the indentation.

Figure 7

A model for how Lmo7 induces apical constriction

In the absence of Lmo7, AJs are undercoated by actomyosin bundles containing mixed polarity cables. Lmo7 recruits NMIIA to AJs and promotes the formation of highly organized actomyosin bundles.

Supplemental information

Supplemental Figure 1

Lmo7 and ZO-1 do not co-localize at AJs in the neuroepithelium

(A) Relative localization of GFP-Lmo7 and RFP-ZO1 in the neuroepithelial cells in *Xenopus* embryos at St 15. An area marked by a dotted rectangle in A is enlarged in B. GFP-Lmo7 forms double-lines at AJs. RFP-ZO1 forms single-lines at AJs. Areas marked by dotted rectangles in A-A" are enlarged in B-B". (B-B") RFP-ZO1 single-lines are located between GFP-Lmo7 double-lines.

Supplemental Figure 2

Lmo7 and α-actinin colocalize at AJs in the superficial ectoderm

(A-A") Relative localization of HA-Lmo7 and α-actinin in the *Xenopus* superficial ectoderm at St 11. An area marked by a dotted rectangle in A is enlarged in B. (B-B") GFP-α-actinin forms double-lines at AJs. HA-Lmo7 double-line overlaps with the GFP- actinin double-line.

Supplemental Figure 3

The expression of GFP-tagged full-length or deletion mutant forms of Lmo7

(A) The expression of GFP-tagged full-length or deletion mutant forms of Lmo7 was confirmed by western blots. (B-F) The accumulation of pigment granules in the superficial ectoderm at St 11. The N-terminal fragment containing the CH domain does not induce pigment granule accumulation (D). The C-terminal coiled-coil domain or the LIM domain does not induce pigment granule accumulation (E,F).

Supplemental Figure 4

The alignment of the evolutionally conserved domain of Lmo7 and LIMCH1

Identical amino acids are labeled by double asterisks. Similar amino acids are labeled by single asterisks. The conserved WQ-WK sequence was mutated in Lmo7(AAAA) mutant protein.

Supplemental Figure 5

The subcellular distribution of GFP-tagged full-length or deletion mutant forms of Lmo7

mRNA encoding GFP-tagged full-length or deletion mutant forms of Lmo7 proteins was injected. The superficial ectoderm in *Xenopus* embryos was co-stained with phalloidin at St 11. All Lmo7 deletion mutants show association with AJs, while the degrees of association vary among these mutants.

Supplemental Figure 6

Lmo7-OE did not increase phosphorylation of MLC

mRNA encoding GFP-Lmo7 was injected into four blastmeres of 4-cell stage embryos. Embryo lysates extracted at St 11 were analyzed by western blots.

Supplemental Figure 7

OE of Lmo7(AAAA) mutant did not increase NMII enrichment at AJs

Lmo7(AAAA) mutant was expressed in mosaic in the *Xenopus* superficial ectoderm. Embryos at St 11 were immunostained by anti-NMIIA antibody.

Supplemental Figure 8

Lmo7 does not substantially increase the accumulation of NMIIB or α-actinin at AJs

(A-A") The subcellular distribution of GFP-NMIIB in the superficial ectoderm of stage 11 *Xenopus* embryos. Areas labeled by rectangles are enlarged in B-B". (B-B") GFP-NMIIB weakly associates with AJs, in addition to localizing in the cytoplasm. (C-C") Effects of Flag-Lmo7 OE on GFP-NMIIB localization at AJs. Flag-Lmo7 was expressed in the subpopulation of GFP-NMIIB expressing cells. Flag-Lmo7 expressing cells are marked by asterisks. Lmo7 OE reduces the cytoplasmic pool of GFP-NMIIB. However, Flag-Lmo7 OE does not increase the intensity of GFP-NMII accumulation at AJs. Areas labeled by rectangles are enlarged in D-D". (D-D") Flag-Lmo7 does not increase GFP-NMIIB

accumulation at AJs. (E-E") Effects of and Flag-Lmo7 OE on GFP-α-actinin localization at AJs. Flag-Lmo7 is expressed in the subpopulation of GFP-α-actinin expressing cells. Flag-Lmo7 expressing cells are marked by asterisks. Flag-Lmo7 OE does not change the intensity of GFP-α-actinin accumulation at AJs. Areas labeled by rectangles are enlarged in E-E". (E-E") Flag-Lmo7 does not increase GFP-α-actinin accumulation at AJs.

References

Abe, K. and Takeichi, M. (2008). EPLIN mediates linkage of the cadherin catenin complex to F-actin and stabilizes the circumferential actin belt. *Proc Natl Acad Sci U S A* **105**, 13-9.

Agarwal, P. and Zaidel-Bar, R. (2019). Principles of Actomyosin Regulation In Vivo. *Trends Cell Biol* **29**, 150-163.

Alvarez, I. S. and Navascues, J. (1990). Shaping, invagination, and closure of the chick embryo otic vesicle: scanning electron microscopic and quantitative study. *Anat Rec* **228**, 315-26.

Amano, M., Ito, M., Kimura, K., Fukata, Y., Chihara, K., Nakano, T., Matsuura, Y. and Kaibuchi, K. (1996). Phosphorylation and activation of myosin by Rho-associated kinase (Rho-kinase). *J Biol Chem* **271**, 20246-9.

Beati, H., Peek, I., Hordowska, P., Honemann-Capito, M., Glashauser, J., Renschler, F. A., Kakanj, P., Ramrath, A., Leptin, M., Luschnig, S. et al. (2018). The adherens junction-associated LIM domain protein Smallish regulates epithelial morphogenesis. *J Cell Biol* **217**, 1079-1095.

Benton, M. A., Frey, N., Nunes da Fonseca, R., von Levetzow, C., Stappert, D., Hakeemi, M. S., Conrads, K. H., Pechmann, M., Panfilio, K. A., Lynch, J. A. et al. (2019). Fog signaling has diverse roles in epithelial morphogenesis in insects. *Elife* **8**.

Beutel, O., Maraspini, R., Pombo-Garcia, K., Martin-Lemaitre, C. and Honigmann, A. (2019). Phase Separation of Zonula Occludens Proteins Drives Formation of Tight Junctions. *Cell* **179**, 923-936 e11.

Bresnick, A. R. (1999). Molecular mechanisms of nonmuscle myosin-II regulation. *Curr Opin Cell Biol* **11**, 26-33.

Chu, C. W., Xiang, B., Ossipova, O., Ioannou, A. and Sokol, S. Y. (2018). The Ajuba family protein Wtip regulates actomyosin contractility during vertebrate neural tube closure. *J Cell Sci* **131**.

Colas, J. F. and Schoenwolf, G. C. (2001). Towards a cellular and molecular understanding of neurulation. *Dev Dyn* **221**, 117-45.

Conti, M. A., Sellers, J. R., Adelstein, R. S. and Elzinga, M. (1991). Identification of the serine residue phosphorylated by protein kinase C in vertebrate nonmuscle myosin heavy chains. *Biochemistry* **30**, 966-70.

Costa, M., Wilson, E. T. and Wieschaus, E. (1994). A putative cell signal encoded by the folded gastrulation gene coordinates cell shape changes during Drosophila gastrulation. *Cell* **76**, 1075-89.

Dahan, I., Yearim, A., Touboul, Y. and Ravid, S. (2012). The tumor suppressor Lgl1 regulates NMII-A cellular distribution and focal adhesion morphology to optimize cell migration. *Mol Biol Cell* **23**, 591-601.

Das, D., Zalewski, J. K., Mohan, S., Plageman, T. F., VanDemark, A. P. and Hildebrand, J. D. (2014). The interaction between Shroom3 and Rho-kinase is required for neural tube morphogenesis in mice. *Biol Open* **3**, 850-60.

Dollar, G. L., Weber, U., Mlodzik, M. and Sokol, S. Y. (2005). Regulation of Lethal giant larvae by Dishevelled. *Nature* **437**, 1376-80.

Drees, F., Pokutta, S., Yamada, S., Nelson, W. J. and Weis, W. I. (2005). Alpha-catenin is a molecular switch that binds E-cadherin-beta-catenin and regulates actin-filament assembly. *Cell* **123**, 903-15.

Du, T. T., Dewey, J. B., Wagner, E. L., Cui, R., Heo, J., Park, J. J., Francis, S. P., Perez-Reyes, E., Guillot, S. J., Sherman, N. E. et al. (2019). LMO7 deficiency reveals the significance of the cuticular plate for hearing function. *Nat Commun* **10**, 1117.

Dulyaninova, N. G., House, R. P., Betapudi, V. and Bresnick, A. R. (2007). Myosin-IIA heavy-chain phosphorylation regulates the motility of MDA-MB-231 carcinoma cells. *Mol Biol Cell* **18**, 3144-55.

Dulyaninova, N. G., Malashkevich, V. N., Almo, S. C. and Bresnick, A. R. (2005). Regulation of myosin-IIA assembly and Mts1 binding by heavy chain phosphorylation. *Biochemistry* **44**, 6867-76.

Eiraku, M., Takata, N., Ishibashi, H., Kawada, M., Sakakura, E., Okuda, S., Sekiguchi, K., Adachi, T. and Sasai, Y. (2011). Self-organizing optic-cup morphogenesis in three-dimensional culture. *Nature* **472**, 51-6.

Elliott, P. R., Irvine, A. F., Jung, H. S., Tozawa, K., Pastok, M. W., Picone, R., Badyal, S. K., Basran, J., Rudland, P. S., Barraclough, R. et al. (2012). Asymmetric mode of Ca(2)(+)-S100A4 interaction with nonmuscle myosin IIA generates nanomolar affinity required for filament remodeling. *Structure* **20**, 654-66.

Even-Faitelson, L. and Ravid, S. (2006). PAK1 and aPKCzeta regulate myosin II-B phosphorylation: a novel signaling pathway regulating filament assembly. *Mol Biol Cell* **17**, 2869-81.

Feng, J., Ito, M., Ichikawa, K., Isaka, N., Nishikawa, M., Hartshorne, D. J. and Nakano, T. (1999). Inhibitory phosphorylation site for Rho-associated kinase on smooth muscle myosin phosphatase. *J Biol Chem* **274**, 37385-90.

Fesenko, I., Kurth, T., Sheth, B., Fleming, T. P., Citi, S. and Hausen, P. (2000). Tight junction biogenesis in the early Xenopus embryo. *Mech Dev* **96**, 51-65.

Garrett, S. C., Varney, K. M., Weber, D. J. and Bresnick, A. R. (2006). S100A4, a mediator of metastasis. *J Biol Chem* **281**, 677-80.

Gates, J. and Peifer, M. (2005). Can 1000 reviews be wrong? Actin, alpha-Catenin, and adherens junctions. *Cell* **123**, 769-72.

Gilmour, D., Rembold, M. and Leptin, M. (2017). From morphogen to morphogenesis and back. *Nature* **541**, 311-320.

Gorfinkiel, N. and Blanchard, G. B. (2011). Dynamics of actomyosin contractile activity during epithelial morphogenesis. *Curr Opin Cell Biol* **23**, 531-9.

Haigo, S. L., Hildebrand, J. D., Harland, R. M. and Wallingford, J. B. (2003). Shroom induces apical constriction and is required for hingepoint formation during neural tube closure. *Curr Biol* **13**, 2125-37.

Hardin, J. and Keller, R. (1988). The behaviour and function of bottle cells during gastrulation of Xenopus laevis. *Development* **103**, 211-30.

Harland, R. M. (1991). In situ hybridization: an improved whole-mount method for Xenopus embryos. *Methods Cell Biol* **36**, 685-95.

Hartsock, A. and Nelson, W. J. (2008). Adherens and tight junctions: structure, function and connections to the actin cytoskeleton. *Biochim Biophys Acta* **1778**, 660-9.

Heissler, S. M. and Sellers, J. R. (2014). Myosin light chains: Teaching old dogs new tricks. *Bioarchitecture* **4**, 169-88.

Hildebrand, J. D. (2005). Shroom regulates epithelial cell shape via the apical positioning of an actomyosin network. *J Cell Sci* **118**, 5191-203.

Hildebrand, J. D. and Soriano, P. (1999). Shroom, a PDZ domain-containing actin-binding protein, is required for neural tube morphogenesis in mice. *Cell* **99**, 485-97.

Ishiyama, N., Sarpal, R., Wood, M. N., Barrick, S. K., Nishikawa, T., Hayashi, H., Kobb, A. B., Flozak, A. S., Yemelyanov, A., Fernandez-Gonzalez, R. et al. (2018). Force-dependent allostery of the alpha-catenin actin-binding domain controls adherens junction dynamics and functions. *Nat Commun* **9**, 5121.

Itoh, K., Ossipova, O. and Sokol, S. Y. (2014). GEF-H1 functions in apical constriction and cell intercalations and is essential for vertebrate neural tube closure. *J Cell Sci* **127**, 2542-53.

Kam, Z., Minden, J. S., Agard, D. A., Sedat, J. W. and Leptin, M. (1991). Drosophila gastrulation: analysis of cell shape changes in living embryos by three-dimensional fluorescence microscopy. *Development* **112**, 365-70.

Kolsch, V., Seher, T., Fernandez-Ballester, G. J., Serrano, L. and Leptin, M. (2007). Control of Drosophila gastrulation by apical localization of adherens junctions and RhoGEF2. *Science* **315**, 384-6.

Lao, D. H., Esparza, M. C., Bremner, S. N., Banerjee, I., Zhang, J., Veevers, J., Bradford, W. H., Gu, Y., Dalton, N. D., Knowlton, K. U. et al. (2015). Lmo7 is dispensable for skeletal muscle and cardiac function. *Am J Physiol Cell Physiol* **309**, C470-9.

Lecuit, T., Lenne, P. F. and Munro, E. (2011). Force generation, transmission, and integration during cell and tissue morphogenesis. *Annu Rev Cell Dev Biol* **27**, 157-84.

Lee, J. D., Silva-Gagliardi, N. F., Tepass, U., McGlade, C. J. and Anderson, K. V. (2007). The FERM protein Epb4.1l5 is required for organization of the neural plate and for the epithelial-mesenchymal transition at the primitive streak of the mouse embryo. *Development* **134**, 2007-16.

Lin, Y. H., Zhen, Y. Y., Chien, K. Y., Lee, I. C., Lin, W. C., Chen, M. Y. and Pai, L. M. (2017). LIMCH1 regulates nonmuscle myosin-II activity and suppresses cell migration. *Mol Biol Cell* **28**, 1054-1065.

Manning, A. J., Peters, K. A., Peifer, M. and Rogers, S. L. (2013). Regulation of epithelial morphogenesis by the G protein-coupled receptor mist and its ligand fog. *Sci Signal* **6**, ra98.

Manning, A. J. and Rogers, S. L. (2014). The Fog signaling pathway: insights into signaling in morphogenesis. *Dev Biol* **394**, 6-14.

Marlow, F., Topczewski, J., Sepich, D. and Solnica-Krezel, L. (2002). Zebrafish Rho kinase 2 acts downstream of Wnt11 to mediate cell polarity and effective convergence and extension movements. *Curr Biol* **12**, 876-84.

Martin, A. C. (2010). Pulsation and stabilization: contractile forces that underlie morphogenesis. *Dev Biol* **341**, 114-25.

Martin, A. C. and Goldstein, B. (2014). Apical constriction: themes and variations on a cellular mechanism driving morphogenesis. *Development* **141**, 1987-98.

Martin, A. C., Kaschube, M. and Wieschaus, E. F. (2009). Pulsed contractions of an actin-myosin network drive apical constriction. *Nature* **457**, 495-9.

Merriam, R. W., Sauterer, R. A. and Christensen, K. (1983). A subcortical, pigment-containing structure in Xenopus eggs with contractile properties. *Dev Biol* **95**, 439-46.

Morita, H., Nandadasa, S., Yamamoto, T. S., Terasaka-Iioka, C., Wylie, C. and Ueno, N. (2010). Nectin-2 and N-cadherin interact through extracellular domains and induce apical accumulation of F-actin in apical constriction of Xenopus neural tube morphogenesis. *Development* **137**, 1315-25.

Murakami, N., Chauhan, V. P. and Elzinga, M. (1998). Two nonmuscle myosin II heavy chain isoforms expressed in rabbit brains: filament forming properties, the effects of phosphorylation by protein kinase C and casein kinase II, and location of the phosphorylation sites. *Biochemistry* **37**, 1989-2003.

Murphy, A. C. and Young, P. W. (2015). The actinin family of actin cross-linking proteins - a genetic perspective. *Cell Biosci* **5**, 49.

Nakajima, H. and Tanoue, T. (2011). Lulu2 regulates the circumferential actomyosin tensile system in epithelial cells through p114RhoGEF. *J Cell Biol* **195**, 245-61.

Nakajima, H. and Tanoue, T. (2012). The circumferential actomyosin belt in epithelial cells is regulated by the Lulu2-p114RhoGEF system. *Small GTPases* **3**, 91-6.

Nishimura, T. and Takeichi, M. (2008). Shroom3-mediated recruitment of Rho kinases to the apical cell junctions regulates epithelial and neuroepithelial planar remodeling. *Development* **135**, 1493-502.

Ooshio, T., Irie, K., Morimoto, K., Fukuhara, A., Imai, T. and Takai, Y. (2004). Involvement of LMO7 in the association of two cell-cell adhesion molecules, nectin and E-cadherin, through afadin and alpha-actinin in epithelial cells. *J Biol Chem* **279**, 31365-73.

Ossipova, O., Kim, K., Lake, B. B., Itoh, K., Ioannou, A. and Sokol, S. Y. (2014). Role of Rab11 in planar cell polarity and apical constriction during vertebrate neural tube closure. *Nat Commun* **5**, 3734.

Pathak, R. and Dermardirossian, C. (2013). GEF-H1: orchestrating the interplay between cytoskeleton and vesicle trafficking. *Small GTPases* **4**, 174-9.

Pellegrin, S. and Mellor, H. (2007). Actin stress fibres. *J Cell Sci* **120**, 3491-9.

Peng, H. B. (1991). Xenopus laevis: Practical uses in cell and molecular biology. Solutions and protocols. *Methods Cell Biol* **36**, 657-62.

Perez-Vale, K. Z. and Peifer, M. (2020). Orchestrating morphogenesis: building the body plan by cell shape changes and movements. *Development* **147**.

Ramkumar, N., Omelchenko, T., Silva-Gagliardi, N. F., McGlade, C. J., Wijnholds, J. and Anderson, K. V. (2016). Crumbs2 promotes cell ingression during the epithelial-to-mesenchymal transition at gastrulation. *Nat Cell Biol* **18**, 1281-1291.

Sakakibara, S., Mizutani, K., Sugiura, A., Sakane, A., Sasaki, T., Yonemura, S. and Takai, Y. (2020). Afadin regulates actomyosin organization through alphaE-catenin at adherens junctions. *J Cell Biol* **219**.

Salbreux, G., Charras, G. and Paluch, E. (2012). Actin cortex mechanics and cellular morphogenesis. *Trends Cell Biol* **22**, 536-45.

Sawyer, J. K., Harris, N. J., Slep, K. C., Gaul, U. and Peifer, M. (2009). The Drosophila afadin homologue Canoe regulates linkage of the actin cytoskeleton to adherens junctions during apical constriction. *J Cell Biol* **186**, 57-73.

Sawyer, J. M., Harrell, J. R., Shemer, G., Sullivan-Brown, J., Roh-Johnson, M. and Goldstein, B. (2010). Apical constriction: a cell shape change that can drive morphogenesis. *Dev Biol* **341**, 5-19.

Schwayer, C., Shamipour, S., Pranjic-Ferscha, K., Schauer, A., Balda, M., Tada, M., Matter, K. and Heisenberg, C. P. (2019). Mechanosensation of Tight Junctions Depends on ZO-1 Phase Separation and Flow. *Cell* **179**, 937-952 e18.

Schwayer, C., Sikora, M., Slovakova, J., Kardos, R. and Heisenberg, C. P. (2016). Actin Rings of Power. *Dev Cell* **37**, 493-506.

Seddiki, R., Narayana, G., Strale, P. O., Balcioglu, H. E., Peyret, G., Yao, M., Le, A. P., Teck Lim, C., Yan, J., Ladoux, B. et al. (2018). Force-dependent binding of vinculin to alpha-catenin regulates cell-cell contact stability and collective cell behavior. *Mol Biol Cell* **29**, 380-388.

Sherrard, K., Robin, F., Lemaire, P. and Munro, E. (2010). Sequential activation of apical and basolateral contractility drives ascidian endoderm invagination. *Curr Biol* **20**, 1499-510.

Shutova, M. S. and Svitkina, T. M. (2018). Mammalian nonmuscle myosin II comes in three flavors. *Biochem Biophys Res Commun* **506**, 394-402.

Sweeton, D., Parks, S., Costa, M. and Wieschaus, E. (1991). Gastrulation in Drosophila: the formation of the ventral furrow and posterior midgut invaginations. *Development* **112**, 775-89.

Takeichi, M. (2014). Dynamic contacts: rearranging adherens junctions to drive epithelial remodelling. *Nat Rev Mol Cell Biol* **15**, 397-410.

Tanaka-Okamoto, M., Hori, K., Ishizaki, H., Hosoi, A., Itoh, Y., Wei, M., Wanibuchi, H., Mizoguchi, A., Nakamura, H. and Miyoshi, J. (2009). Increased susceptibility to spontaneous lung cancer in mice lacking LIM-domain only 7. *Cancer Sci* **100**, 608-16.

Terry, S. J., Zihni, C., Elbediwy, A., Vitiello, E., Leefa Chong San, I. V., Balda, M. S. and Matter, K. (2011). Spatially restricted activation of RhoA signalling at epithelial junctions by p114RhoGEF drives junction formation and morphogenesis. *Nat Cell Biol* **13**, 159-66.

Vicente-Manzanares, M., Ma, X., Adelstein, R. S. and Horwitz, A. R. (2009). Non-muscle myosin II takes centre stage in cell adhesion and migration. *Nat Rev Mol Cell Biol* **10**, 778-90.

Wallingford, J. B., Niswander, L. A., Shaw, G. M. and Finnell, R. H. (2013). The continuing challenge of understanding, preventing, and treating neural tube defects. *Science* **339**, 1222002.

Weiser, D. C., Row, R. H. and Kimelman, D. (2009). Rho-regulated myosin phosphatase establishes the level of protrusive activity required for cell movements during zebrafish gastrulation. *Development* **136**, 2375-84.

Williams, M., Burdsal, C., Periasamy, A., Lewandoski, M. and Sutherland, A. (2012). Mouse primitive streak forms in situ by initiation of epithelial to mesenchymal transition without migration of a cell population. *Dev Dyn* **241**, 270-83.

Yamada, S., Pokutta, S., Drees, F., Weis, W. I. and Nelson, W. J. (2005). Deconstructing the cadherin-catenin-actin complex. *Cell* **123**, 889-901.

Yamashita, S., Tsuboi, T., Ishinabe, N., Kitaguchi, T. and Michiue, T. (2016). Wide and high resolution tension measurement using FRET in embryo. *Sci Rep* **6**, 28535.

Yonemura, S., Itoh, M., Nagafuchi, A. and Tsukita, S. (1995). Cell-to-cell adherens junction formation and actin filament organization: similarities and differences between non-polarized fibroblasts and polarized epithelial cells. *J Cell Sci* **108 (Pt 1)**, 127-42.

Yonemura, S., Wada, Y., Watanabe, T., Nagafuchi, A. and Shibata, M. (2010). alpha-Catenin as a tension transducer that induces adherens junction development. *Nat Cell Biol* **12**, 533-42.

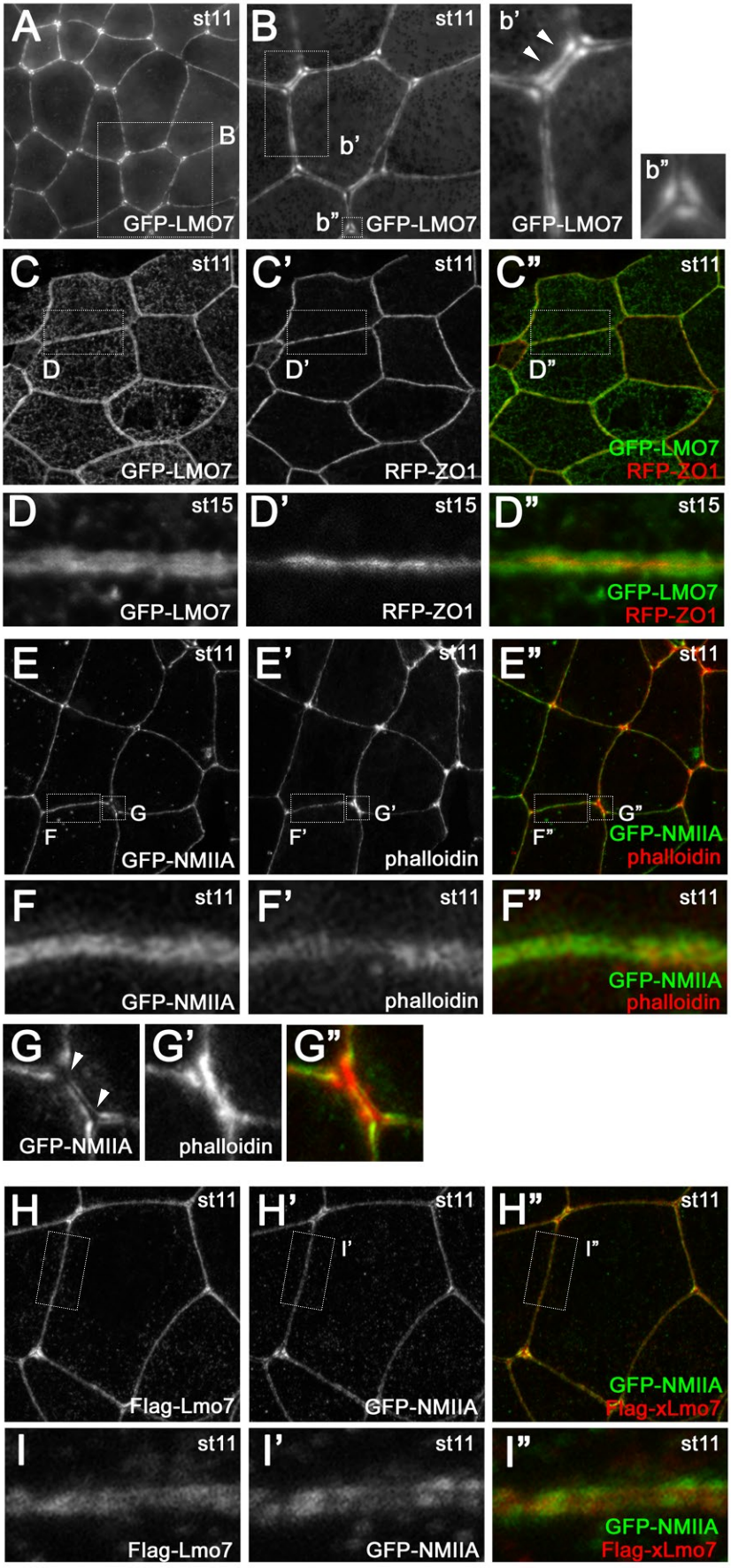

Figure 1

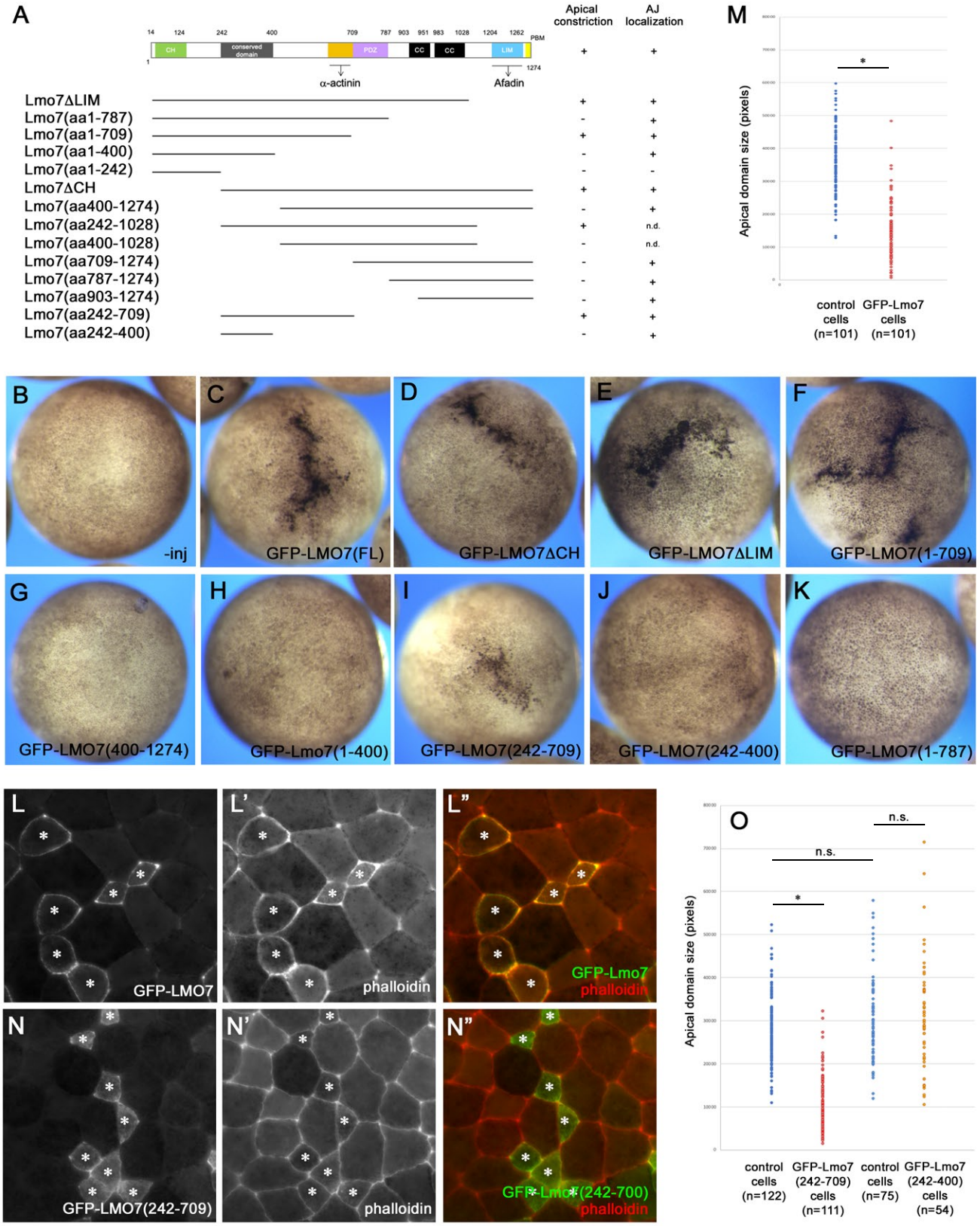

Figure 2

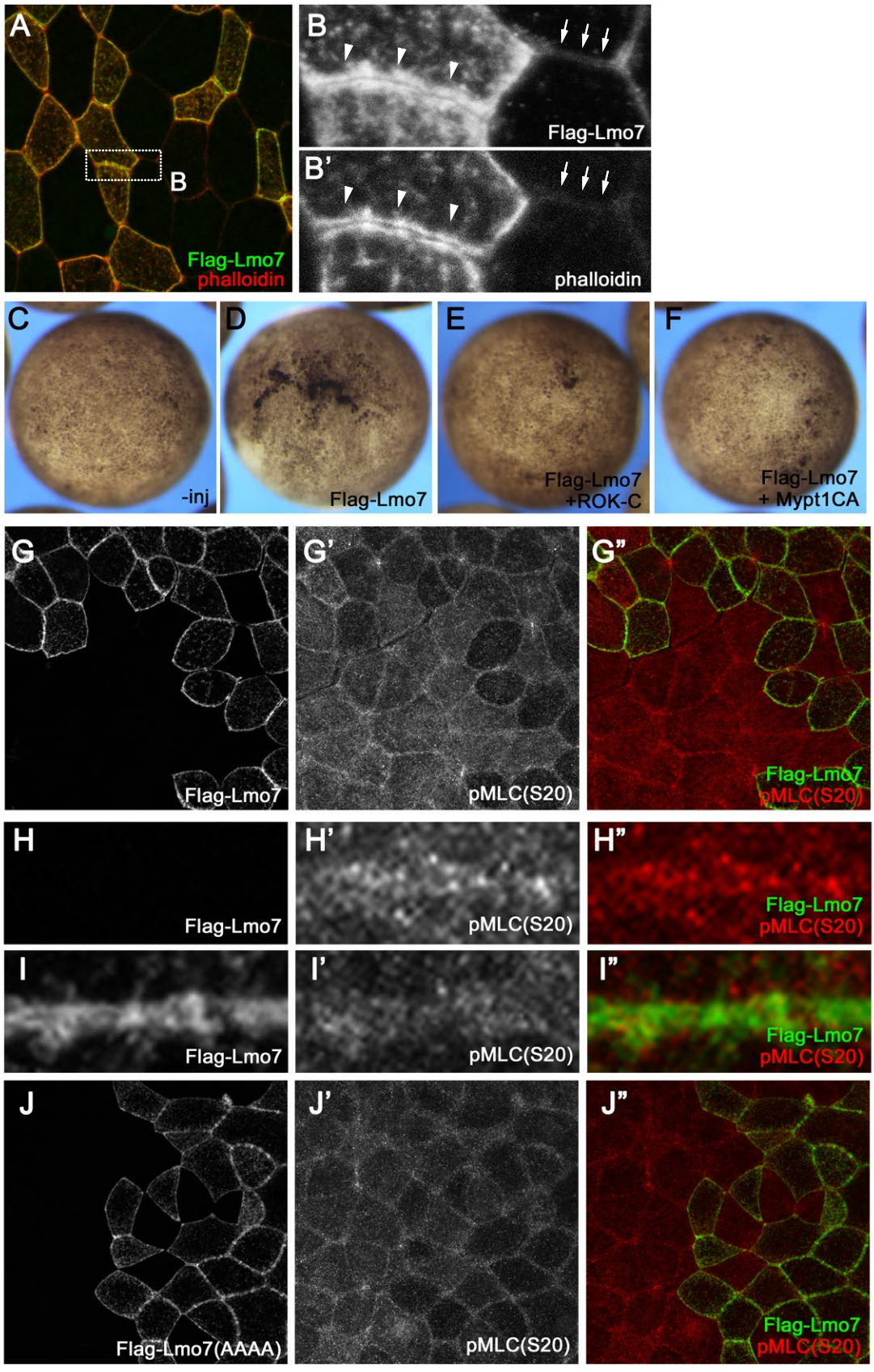

Figure 3

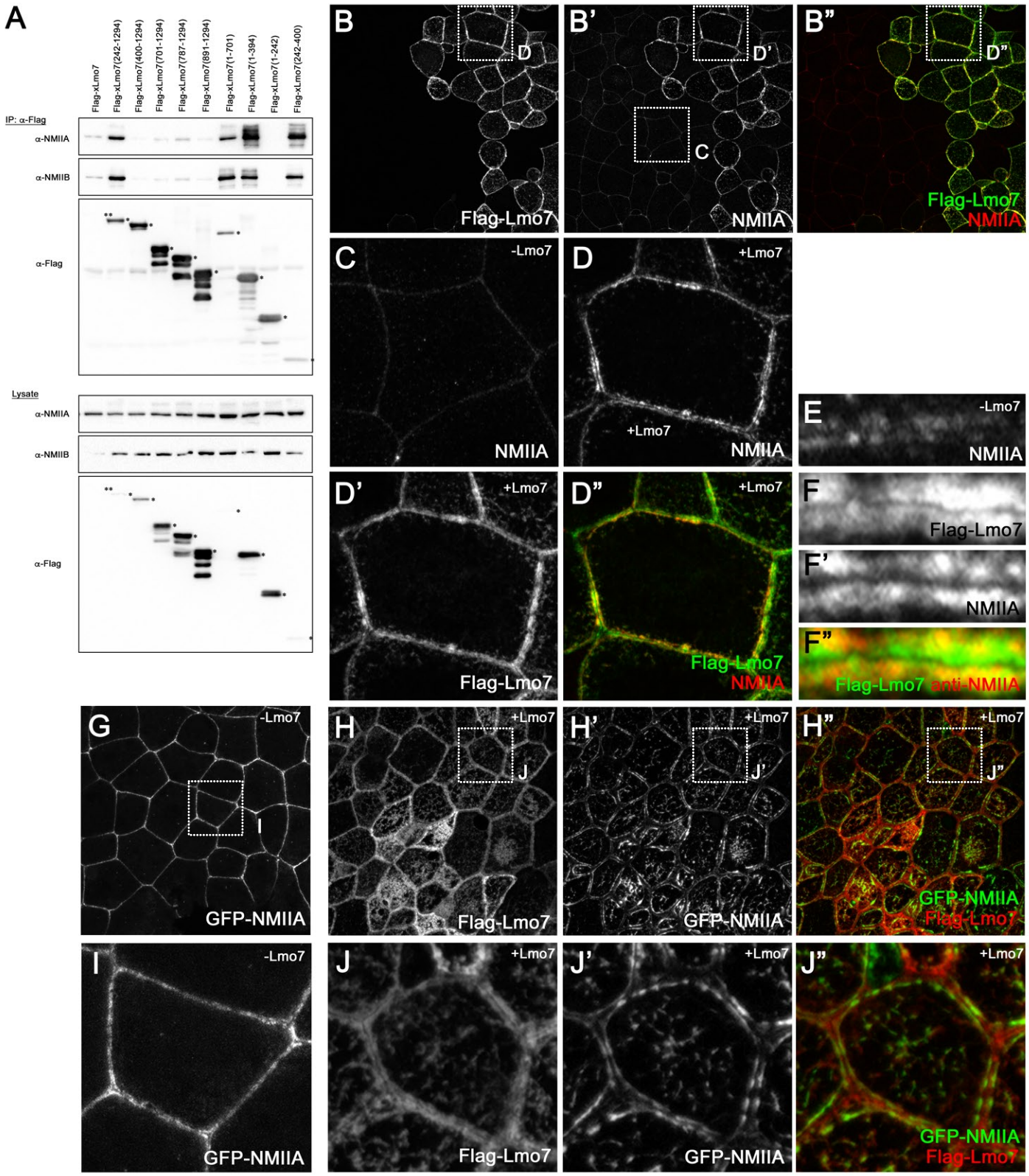

Figure 4

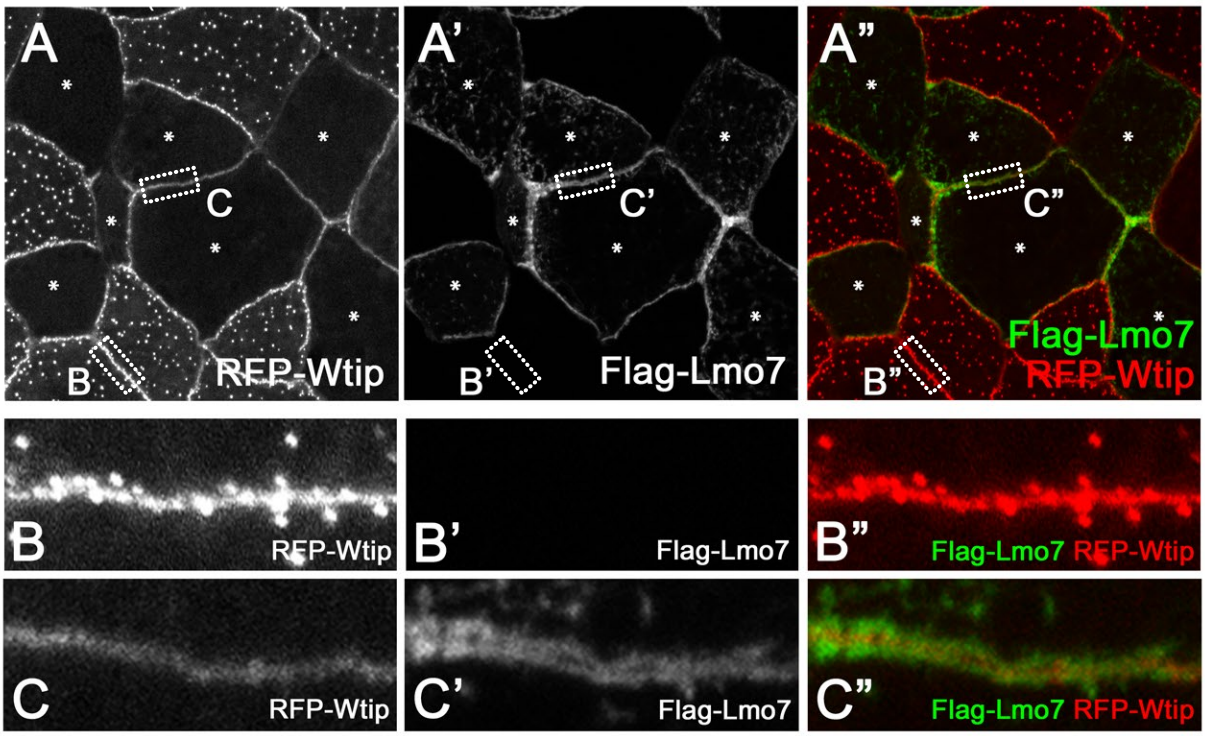

Figure 5

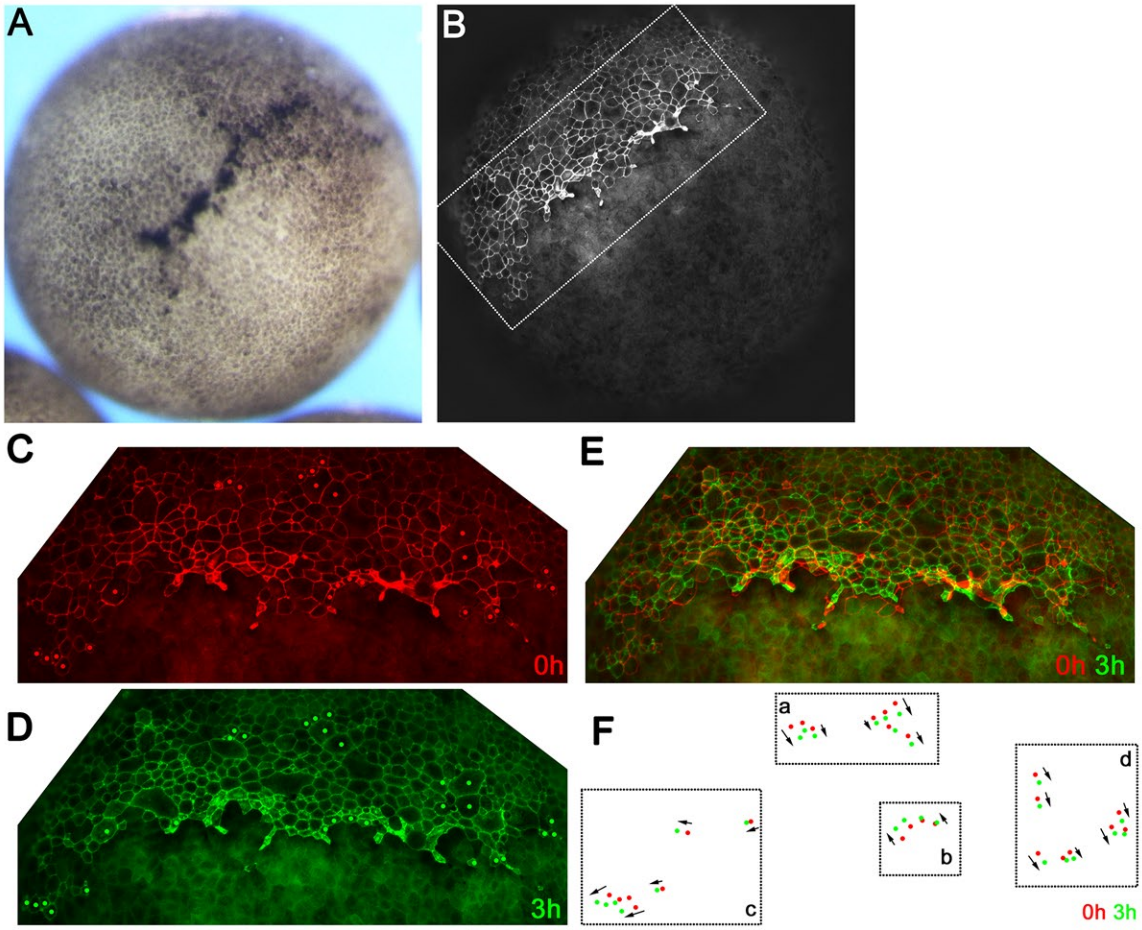

Figure 6

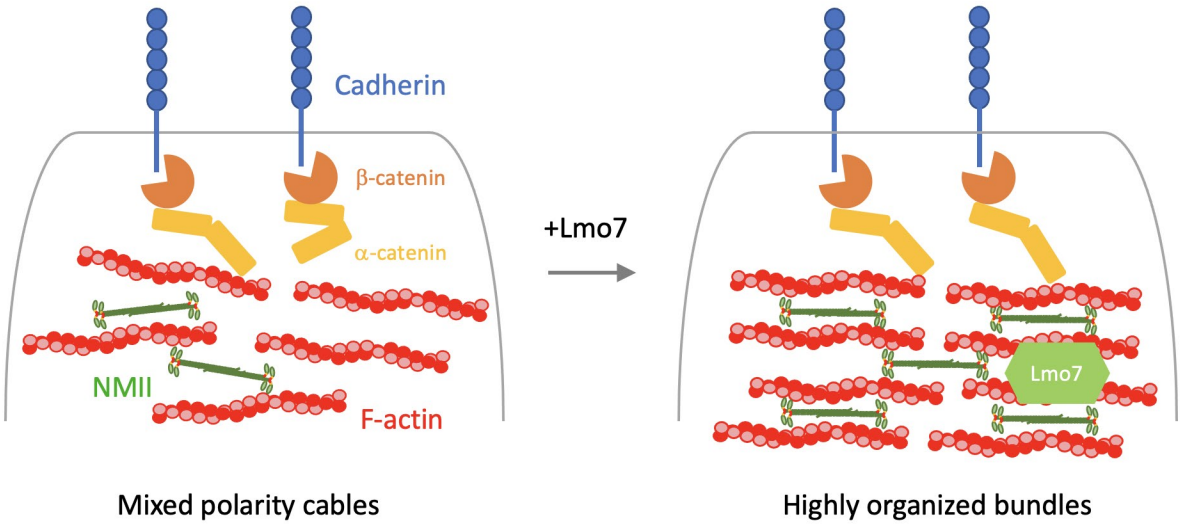

Figure 7

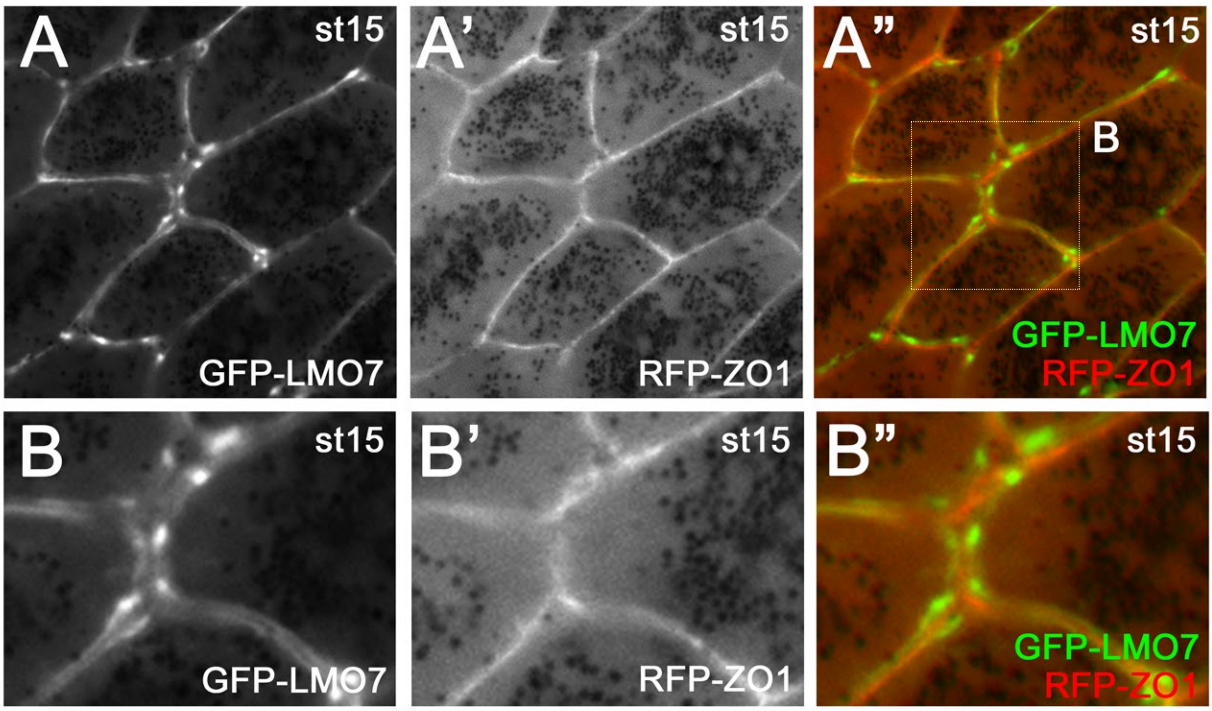

Figure S1

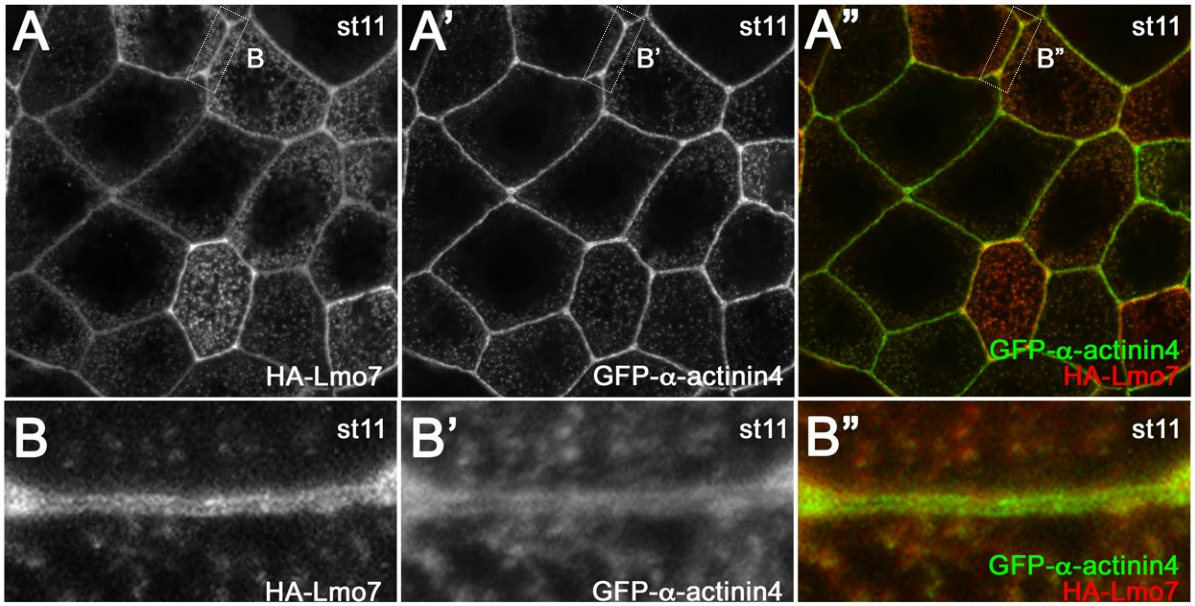

Figure S2

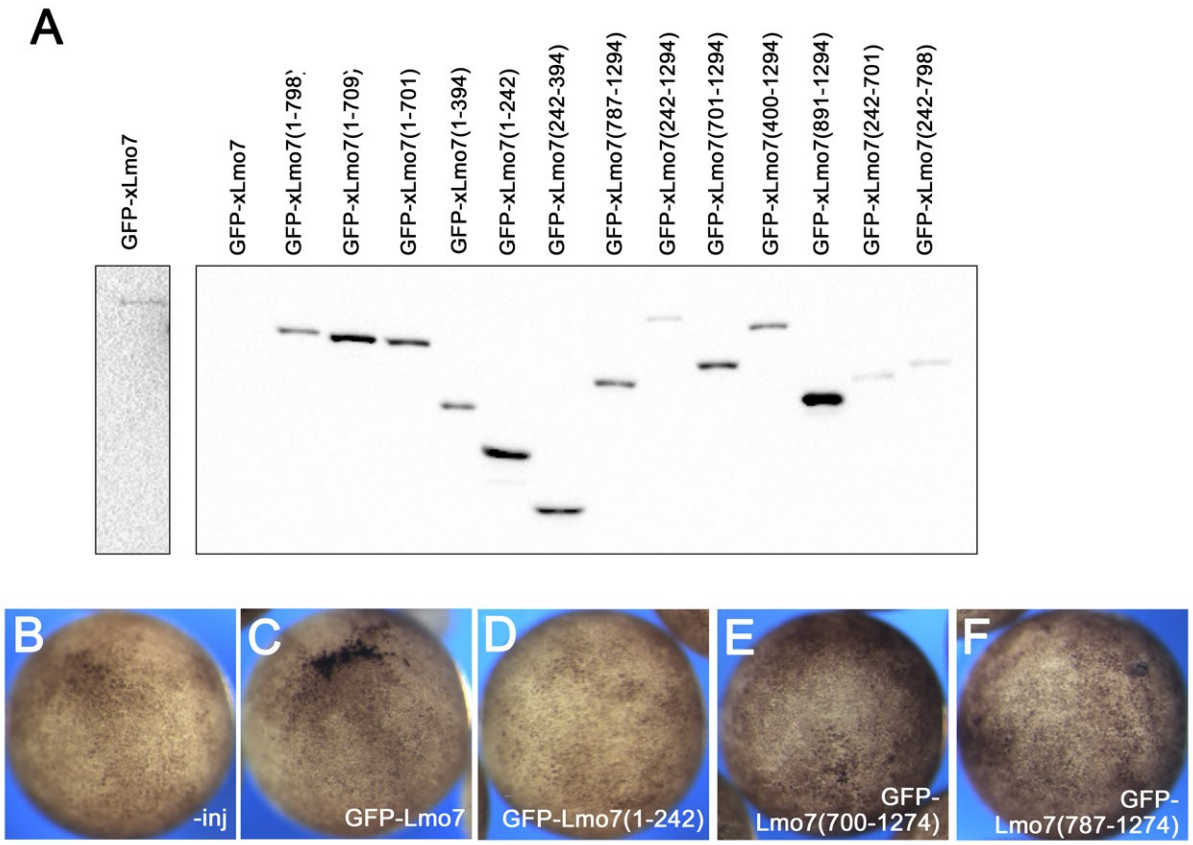

Figure S3

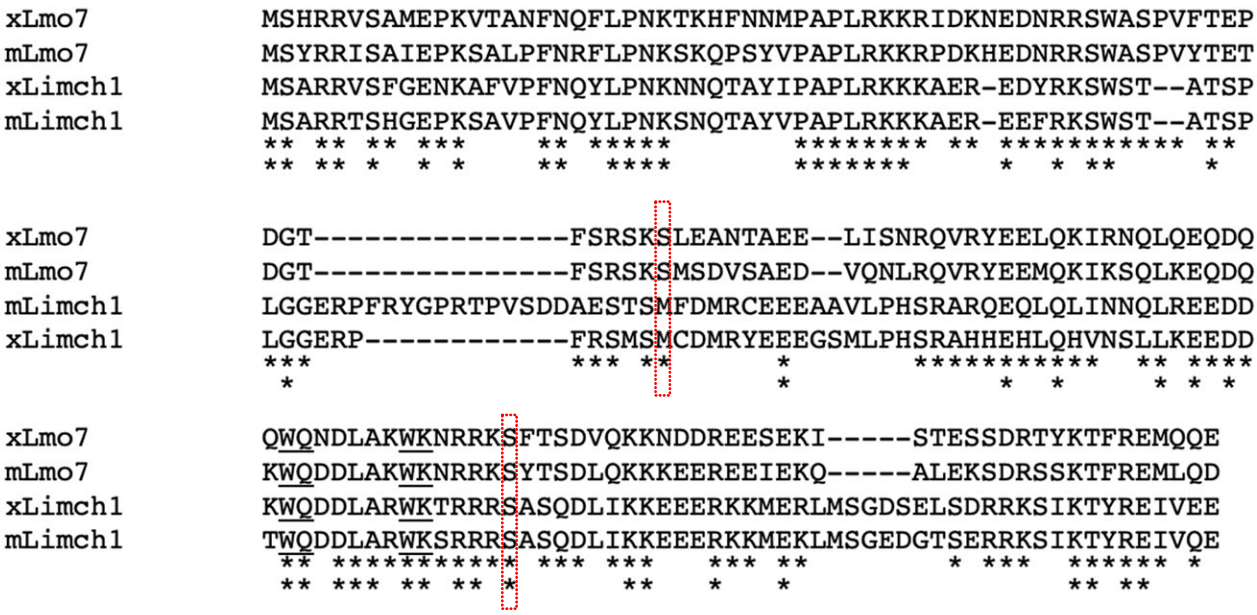

Figure S4

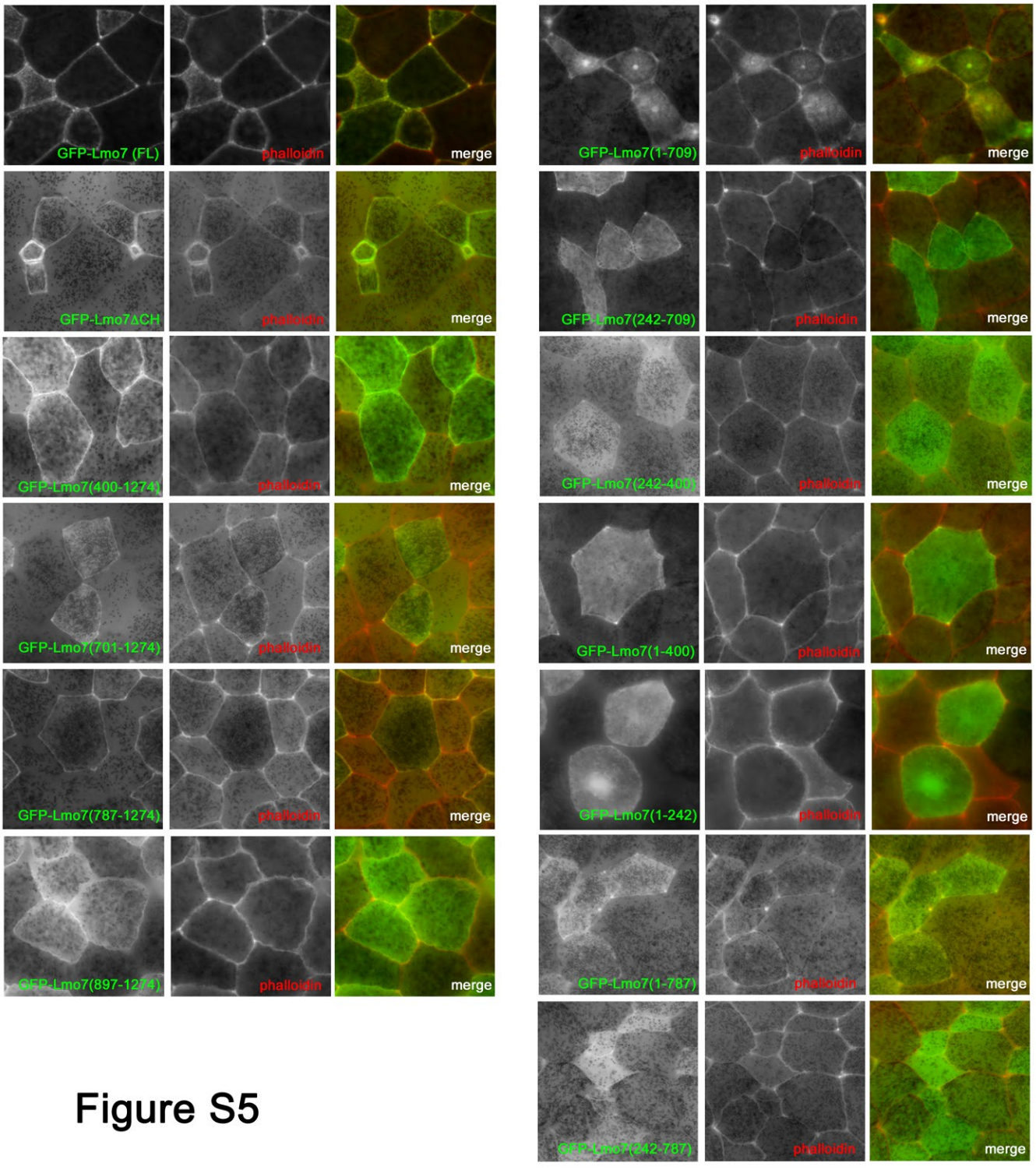

Figure S5

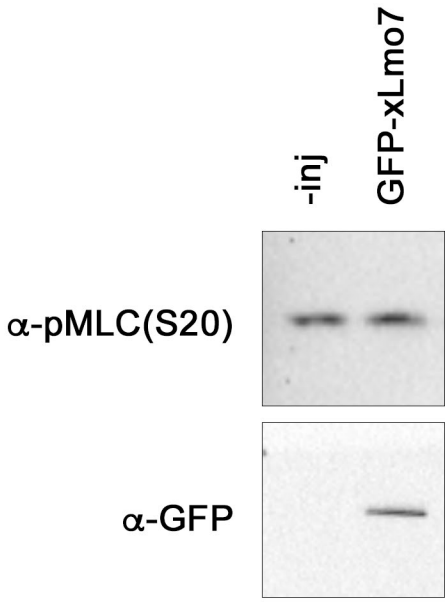

Figure S6

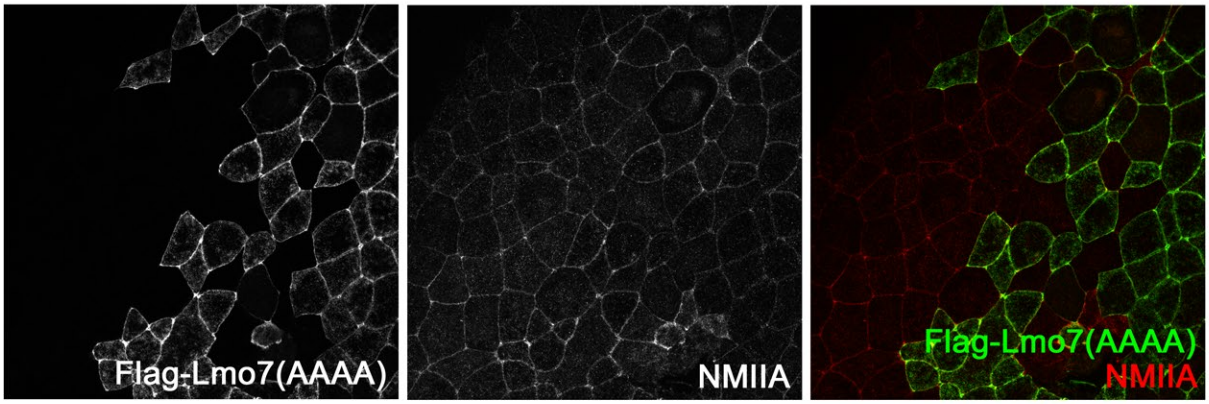

Figure S7

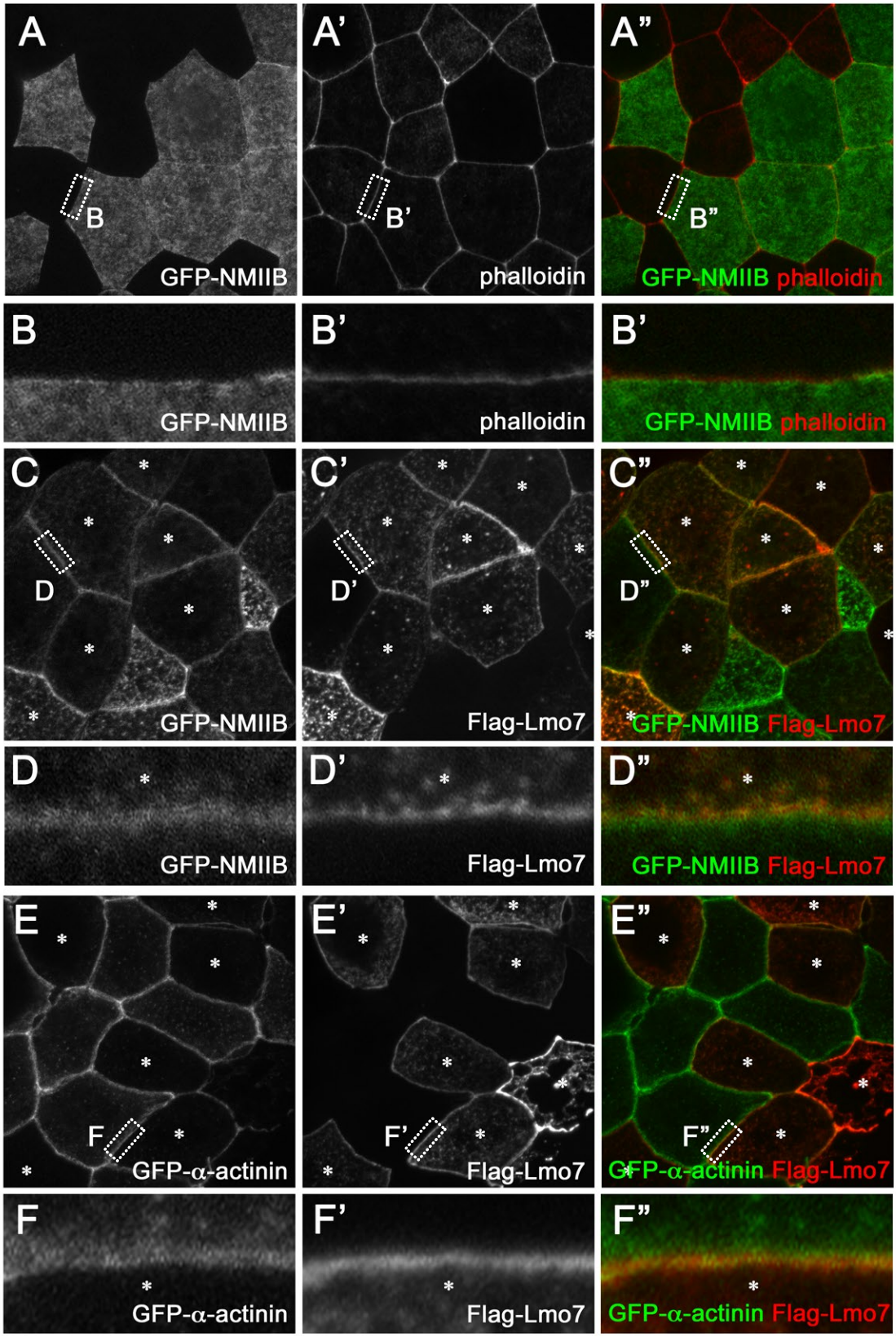

Figure S8

Primer list

xLmo7-2F-EcoRI	gaattcggaatggaatgaaaattc
xLmo7-242F-EcoRI	gaattccatgtcccatcgtagg
xLmo7-400F-EcoRI	gaattcggagagggaaacccg
xLmo7-700F-EcoRI	gaattcgtacagtgacctgagaat
xLmo7-787F-EcoRI	gaattctggcaagaatgactgg
xLmo7-898F-EcoRI	gaattcttgggatccagaaga
xLmo7-242R-stop-NheI	gctagctcagtcatctttgctgctg
xLmo7-394R-stop-NheI	gctagctcaggtttccctctcctgt
xLmo7-709R-stop-NheI	gctagctcaaggtttctggttaatgc
xLmo7-790R-stop-NheI	gctagctcagtcattcttgccatatc
xLmo7-1028R-stop-NheI	gctagctcattttaaaacattattcctttgtc
xLmo7-1274R-stop-NheI	gctagctcacatggaggttgg
xLmo7-WQWK(AAAA)-F	gagcaggatcagcagGCgGCgaatgatttagcaaaaGCgGCgaatcgtcgaaaaagc
xLmo7-WQWK(AAAA)-R	gctttttcgacgattcGCcGCtttgctaaatcattcGCcGCctgctgatcctgctc

Supplemental table 1